6. SITE 1042[1]

Shipboard Scientific Party[2]

HOLE 1042A

Position: 9°39.352′N, 86°06.760′W

Start hole: 1345 hr, 1 December 1996

End hole: 0715 hr, 4 December 1996

Time on hole: 54.75 hr (2.28 days)

Seafloor (drill-pipe measurement from rig floor, mbrf): 3605.0

Water depth (drill-pipe measurement from sea level, m): 3593.8

Distance between rig floor and sea level (m): 11.2

Total depth (drill-pipe measurement from rig floor, mbrf): 3845.1

Penetration (mbsf): 240.1

Coring totals:

Type: RCB; No: 7; Cored: 66.7 m; Recovered: 12.85 m (19.3%)

Formation:

Subunit 1A (48.7–163.3 mbsf): Olive gray silty claystone (late Miocene–?late Pleistocene)

Subunit 1B (201.7–240.1 mbsf): Dark olive green silty claystone with beds of light yellowish gray limestone (middle Miocene?–late Miocene)

HOLE 1042B

Position: 9°39.334′N, 86°06.739′W

Start hole: 0715 hr, 4 December 1996

End hole: 0400 hr, 8 December 1996

Time on hole: 92.75 hr (3.87 days)

Seafloor (drill-pipe measurement from rig floor, mbrf): 3592.5

Water depth (drill-pipe measurement from sea level, m): 3581.2

Distance between rig floor and sea level (m): 11.3

Total depth (drill-pipe measurement from rig floor, mbrf): 3983.3

Penetration (mbsf): 390.8

Drilled: 316 m

Coring totals:

Type: RCB; No: 8; Cored: 74.8 m; Recovered: 8.89 m (11.9%)

Formation:

Subunit 2A (316.0–342.9 mbsf): Light gray carbonate-cemented sandstone and sandstone breccia (early–middle Miocene)

Subunit 2B (342.9–353.7 mbsf): Green to grayish green breccia with clasts of doleritic basalt, chert, sandstone, siltstone, and claystone (early–middle Miocene)

Subunit 1B* (353.7–390.8 mbsf): Dark olive green silty claystone with clasts of light yellowish gray limestone (early/middle–late Miocene)

HOLE 1042C

Position: 9°39.315′N, 86°06.722′W

Start hole: 0345 hr, 13 December 1996

End hole: 2200 hr, 14 December 1996

Time on hole: 42.25 hr (1.76 days)

Seafloor (drill-pipe measurement from rig floor, mbrf): 3585.0

Water depth (drill-pipe measurement from sea level, m): 3573.6

Distance between rig floor and sea level (m): 11.4

Total depth (drill-pipe measurement from rig floor, mbrf): 3882.6

Penetration (mbsf): 297.6

Logging while drilling

Principal results: The prime objective of Site 1042 was to determine the nature and composition of the prism material underlying the slope apron. A fundamental question to answer was whether the underlying prism rocks formed by offscraping or underplating of the incoming strata of the Cocos Plate, or whether it represents material from or continuous with the adjacent onshore rocks in Costa Rica, as seen on the Nicoya Peninsula. Additional objectives included an understanding of the fluid-flow regime of the midslope, and a comparison of the apron material with that of the deformed sedimentary wedge above the décollement, drilled at Site 1040. An additional objective was to obtain high-quality in situ measurements using logging-while-drilling (LWD) technology.

Our objective of sampling the prism beneath the apron was not realized at Site 1041 because of difficult hole conditions. For that reason we obtained permission to drill Site 1042, located closer to the trench in a spot where the prism reflector occurred 200 m shallower than that at Site 1041, at an estimated depth of about 300 mbsf. Our objective at Site 1042 was primarily to reach the prism reflector.

We succeeded in reaching and coring the high-amplitude reflection marking the top of the prism. Spot coring every 50 m showed a sedimentary section similar to the deeper parts of Site 1041, although additional careful study will be necessary to make any detailed comparisons. We subdivided the sedimentary section into two subunits on the basis of lithologic and age differences: Subunits 1A and 1B (Fig. 1). Subunit 1A (48.7–163.3 mbsf) consists mostly of silty claystone, including ubiquitous volcanic glass with common to trace amount of microfossils. Subunit 1A is late Pleistocene?–middle Miocene in age on the basis of planktonic foraminifers. Subunit 1B (201.7–240.1 mbsf) is composed dominantly of silty claystone and limestone with matrix-supported breccia. Thin layers of glauconitic sandstone were recognized also. Subunit 1B is middle–late Miocene? in age, which was determined from common well-preserved foraminifers with few to trace amounts of nannofossils and diatoms.

At 316 mbsf, we cored a carbonate-cemented breccia (Subunit 2A), consisting of angular to subangular sandstone clasts and other clasts that have not yet been analyzed. Between 342.9 and 353.7 mbsf, we recovered breccia composed of fragments of red chert, doleritic basalt, and altered

[1]Kimura, G., Silver, E.A., Blum, P., et al., 1997. *Proc. ODP, Init. Repts.*, 170: College Station, TX (Ocean Drilling Program).

[2]Shipboard Scientific Party is given in the list preceding the Table of Contents.

Previous Chapter Table of Contents Next Chapter

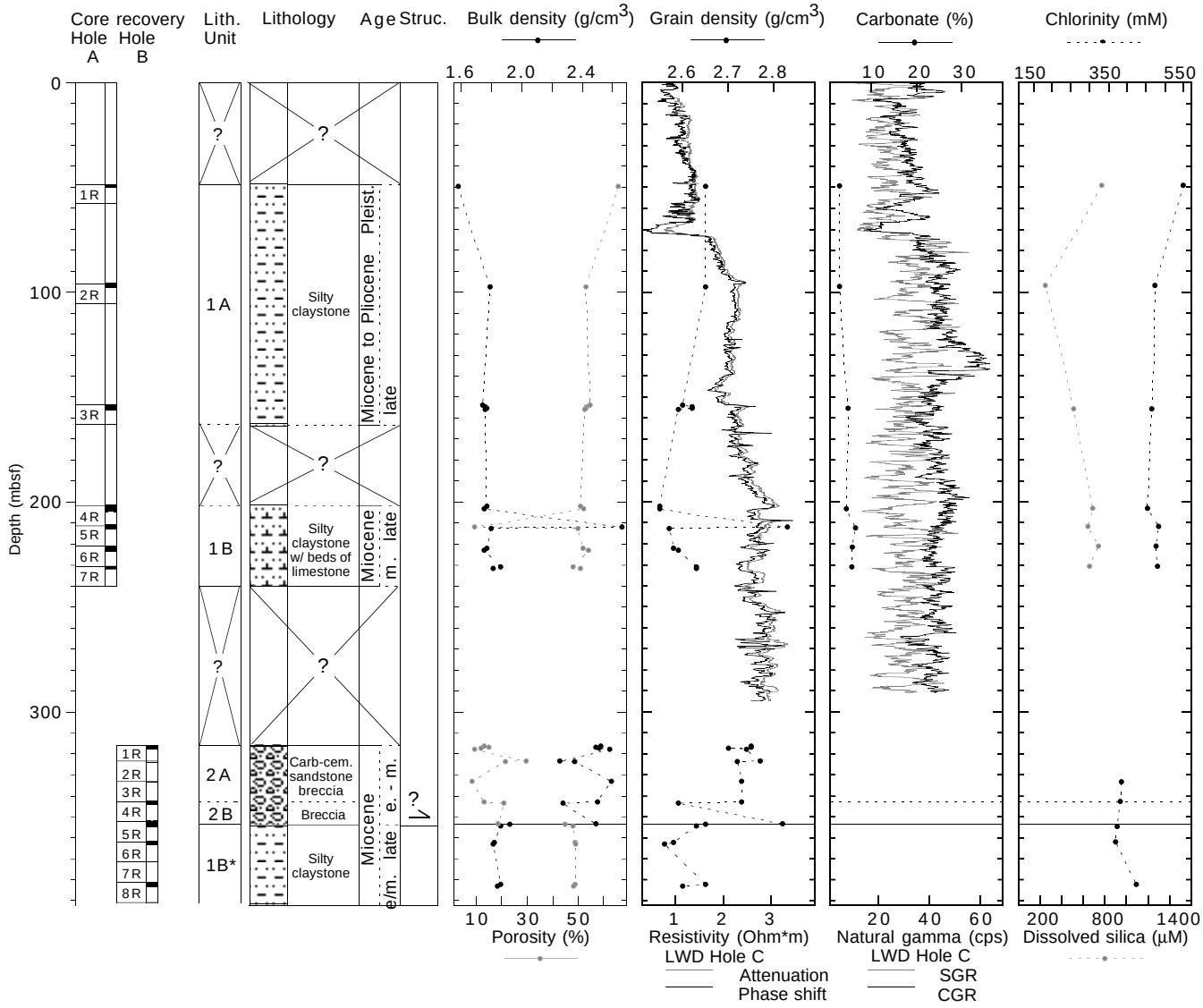

Figure 1. Graphical representation and summary plots of shipboard core and downhole measurements. Explanation of data types and their acquisition are found in the "Explanatory Notes" chapter. Shipboard descriptions of data are found in relevant sections in this chapter. LWD = logging while drilling, SGR = spectral gamma ray (total counts), and CGR = computed gamma ray (total counts minus contribution of uranium).

mafic rock, sandstone, siltstone, and claystone, with a clayey silt matrix (Subunit 2B). Some of these rocks are similar to outcrops described onshore. The carbonate-cemented sandstone breccia has a density and sound velocity of ~2 g/cm^3 and 4.6 km/s, respectively, which explains both the high-amplitude reflection at the top of the prism and the velocities obtained from ocean-bottom seismometer (OBS) and ocean-bottom hydrophone (OBH) refraction data. Preliminary age determination on both breccias is early–middle Miocene. Beneath the breccia is silty claystone of Subunit 1B*, dated at early/middle–late Miocene, and the contact thrust is interpreted as a fault.

Objectives of the geochemistry program at Site 1042 were similar to those at Site 1041. Additional chemistry at Site 1042 was needed to tie in these observations with those at other sites. In this light, the work was a success. Because coring was done only every 50 m until 200 mbsf, all of the pore-fluid samples analyzed were from beneath the sulfate-reduction zone; therefore methane concentrations have high values even in the shallowest sample analyzed, at ~50 mbsf. The section drilled lies within the stability field of methane hydrate, and mild gas escape was observed in the few sediment samples obtained from ~100 to 230 mbsf. This effect is most likely responsible for at least some of the C_1 freshening also encountered at this site. An abrupt increase in the content of C_1 through C_3 and traces of higher hydrocarbons through C_6 were observed between 150 and 200 mbsf where a major fault was intersected, suggesting that they formed at >100°C. A change in the pore-fluid chemistry occurs at ~100 mbsf; below 100 mbsf and crossing a major fault to ~230 mbsf, the chemistry is roughly constant with characteristics similar to those observed at Site 1041 beneath the fluid conduit at 280–300 mbsf, and at Site 1040 beneath the conduit at ~180 mbsf. These characteristics include elevated Ca concentration and both Cl concentration and Na/Cl values that are lower than seawater.

Downhole logging acquired resistivity and gamma-ray logs with the compensated dual resistivity (CDR) tool. A major break in resistivity occurs in the interval between 67 and 74 mbsf. This change in resistivity roughly coincides with the location of a normal fault in the seismic-reflection records. A large increase in resistivity occurs at 145 mbsf, and below that resistivity values increase gradually with depth. A number of small peaks could represent gas hydrates.

In summary, even though this site was spot-cored for the first 200 mbsf, it was highly successful in meeting one of the major objectives of Leg 170—determining something about the physical nature of the top of

the prism. Together with Site 1041, the sites through the apron have provided a nearly complete picture of mid-slope geology. These sites have clarified the environment and character of the gas hydrates, the pathways of fluid flow, and the sources of the fluids moving through the apron and prism. Both physical properties data and downhole measurements using LWD have also contributed in important ways to this knowledge. The primary goal of drilling through the apron, to understand the nature of the prism material below, has been met.

BACKGROUND AND SCIENTIFIC OBJECTIVES

Site 1042 was located at the seaward edge of the high-amplitude, top-of-prism reflection (Fig. 2). The purpose of drilling Site 1042 was the failure of Site 1041 to reach the prism objective because of drilling problems. We chose Site 1042 because the depth to the reflective, top-of-prism surface is about 200 m shallower than anywhere else within the three-dimensional (3-D) seismic survey. Careful analysis of the 3-D seismic data at that point and throughout the lower slope region of 3-D coverage showed that the point chosen was truly part of the widespread reflective surface that had been mapped continuously throughout the 3-D survey. For that reason we were confident that a successful entry into the reflective, top-of-prism surface would yield materials indicative of that surface and the upper level of the prism.

In the area of Site 1042, the top-of-prism reflection is cut by numerous faults, most likely thrust faults because the surface is often duplicated and shows evidence of thickening (Fig. 3). To this extent the structure at Site 1042 is similar to that at Site 1041, which is also cut by numerous thrust faults. Additional processes are active at Site 1042, however. A possible reason for the relative uplift of the top-of-prism reflector in the southeast corner of the 3-D survey area is the presence of a horst block on the underthrusting Cocos Plate beneath this zone of uplift. The horst block on the lower plate is closely related spatially to the zone of uplift of the top-of-prism reflection (Shipley et al., 1992).

Further structural complications are noted near Site 1042. The seafloor in the vicinity of this site is marked by a number of closely spaced escarpments, downthrown to the southwest. Associated with these scarps are a set of down to the southwest directed reflections,

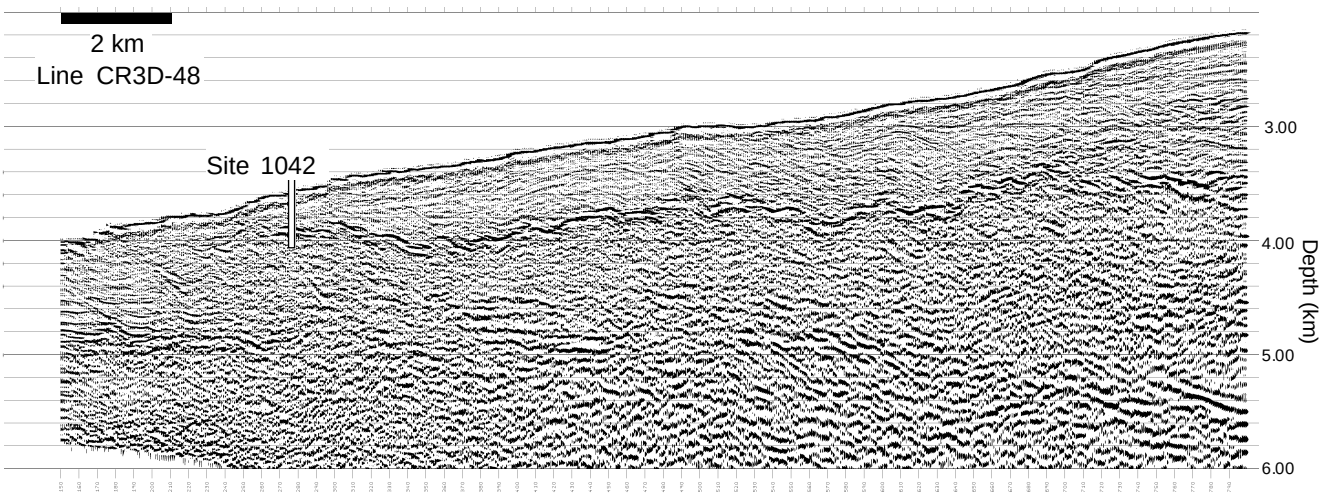

Figure 2. Line CR3D-48, crossing Site 1042. This profile images the top-of-prism reflection, which decreases in depth beneath the seafloor downslope. Farther upslope the surface gets progressively deeper and downslope it apparently disappears.

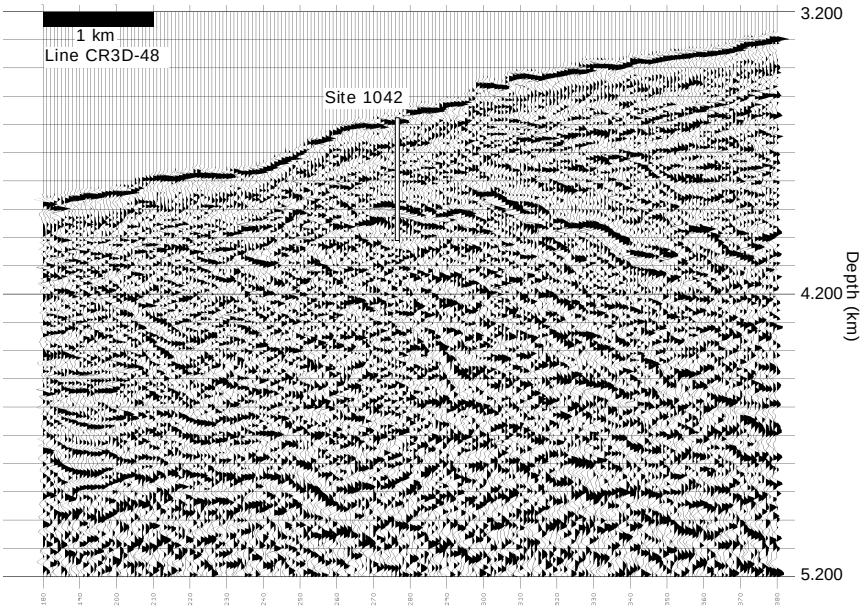

Figure 3. Close-up of Line CR3D-48, centered at Site 1042, imaging the apparent displacement on normal faults near the surface and thrust faults within the underlying prism.

which could represent reflections from fault surfaces. If so, then these escarpments are most likely formed as a result of normal faulting at the surface. How do the normal faults and thrust faults interact? One interpretation is that the passage of the horst results in uplift and steepening of this part of the slope, probably involving some thickening caused by thrust faulting. The steepened slopes fail through sliding, forming the normal fault scarps, a process that thins the apron sequence above the top-of-prism reflector. At a smaller scale, this process is analogous to deformation associated with seamount subduction (Lallemand and Le Pichon, 1987; Lallemand et al., 1992). In addition, it is likely that the apron section also thins downslope, as we note a definite trend of downslope thinning on all the seismic lines (Fig. 2). Seismic cross-line CR3D–276 (Fig. 4) shows complexity in the cross-line direction as well. It also shows that Site 1042 is located near the southeast edge of the 3-D data set.

OPERATIONS

Hole 1042A

The ship proceeded in dynamic positioning (DP) mode from Site 1041 to Site 1042. The pipe was tripped to a depth of 3529.0 m, where the water-sampling temperature probe (WSTP) and APC temperature tools were deployed for a bottom-water sample and temperature measurement. After recovering the WSTP assembly, a center bit was dropped, and the pipe was lowered slowly while "feeling" for bottom. The corrected precision depth recorder (PDR) depth of 3529.0 m was thought to be inaccurate because of the seafloor geometry. Seismic survey data corrected to the rig floor indicated that the seafloor should be at ~3589.4 m. Bottom was tagged with the drill pipe at 3605.0 m, and this depth was used as the official seafloor depth.

Drilling proceeded to a depth of 48.7 mbsf, where the center bit was recovered and a rotary core barrel (RCB) was dropped. Permission had been received to allow spot coring of this hole in 50-m increments to a depth of ~200 mbsf. RCB cores were recovered from depths of 48.7–57.8 mbsf (Core 170-1042A-1R), 96.1–105.7 mbsf (Core 2R), and 153.7–163.3 mbsf (Core 3R; Tables 1, 2). Core recovery was poor, as is often the case during spot-coring operations. A RCB center-bit assembly was used for the drilled intervals between cores. DVTP temperature measurements were attempted after Cores 1R and 2R, but the data were bad.

Continuous RCB coring began with Core 4R at a depth of 201.8 mbsf and continued through Core 7R to a depth of 3845.1 m (240.1 mbsf). Cores 6R and 7R were cut with 300–400 psi, which marked the beginning of hole problems that were never corrected. A total of 12 hr was spent conducting remedial work on the hole. Wiper trips, hole sweeps with sepiolite and Quick Sweep material, and washing and reaming were all tried, but to no avail. Stalling torque, persistent back pressure, and a general inability to clean the hole eventually led to abandonment of further drilling attempts at a total depth of 240.1 mbsf, which was short of the desired 325 mbsf objective. The cause of the hole trouble was believed to be the inability to properly clean the hole of cuttings (lost circulation), aggravated by formation overpressure and a high-angle fault zone at ~180 mbsf.

Table 1. Coring summary for Site 1042.

Core	Date (Dec. 1996)	Time (UTC)	Depth (mbsf)	Length cored (m)	Length recovered (m)	Recovery (%)
170-1042A-						
1R	02	1215	48.7-57.8	9.1	1.25	13.7
2R	02	1900	96.1-105.7	9.6	1.65	17.2
3R	03	0135	153.7-163.3	9.6	2.60	27.1
4R	03	0625	201.7-211.3	9.6	2.26	23.5
5R	03	1025	211.3-220.9	9.6	1.62	16.9
6R	03	1310	220.9-230.5	9.6	2.30	23.9
7R	03	1530	230.5-240.1	9.6	1.17	12.2
Coring totals:				66.7	12.85	19.3
170-1024B-						
1R	07	0225	316.0-323.5	7.5	1.77	23.6
2R	07	0415	323.5-333.1	9.6	0.47	4.9
3R	07	0615	333.1-342.7	9.6	0.13	1.4
4R	07	0955	342.7-352.3	9.6	0.78	8.1
5R	07	1230	352.3-361.9	9.6	2.19	22.8
6R	07	1445	361.9-371.5	9.6	1.26	13.1
7R	07	1750	371.5-381.2	9.7	0.00	0.0
8R	07	2150	381.2-390.8	9.6	2.29	23.8
Coring totals:				74.8	8.89	11.9

Note: UTC = Universal Time Coordinated.

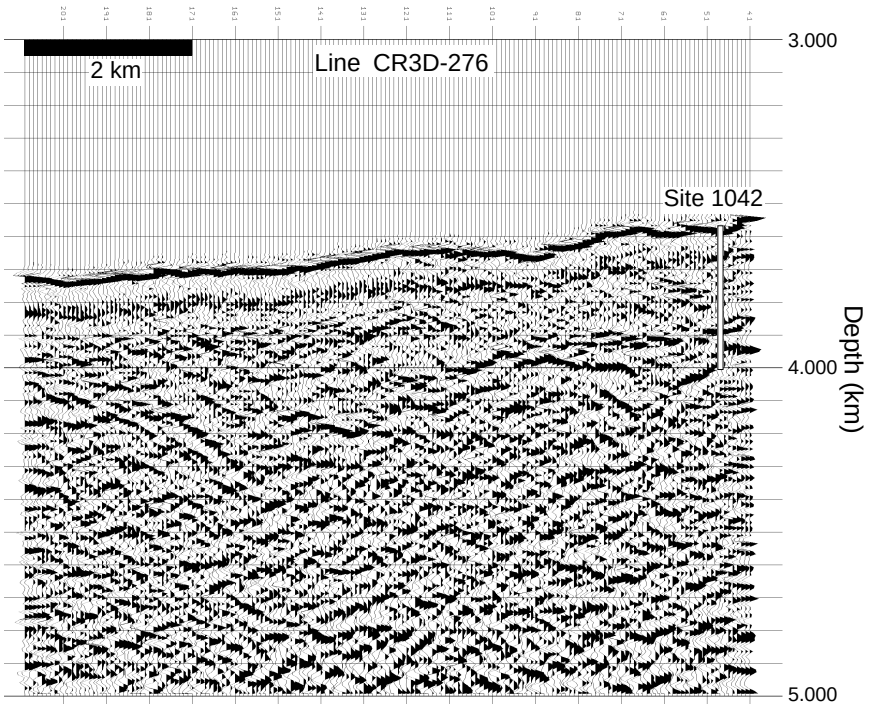

Figure 4. Seismic-reflection cross-line CR3D-276, crossing Site 1042. Note that the site is located close to the southeast edge of the survey.

Table 2. Coring section summary for Site 1042.

Leg	Site	Hole	Core	Type	Top (mbsf)	Bottom (mbsf)	Advancement	Section number	Liner length (m)	Curated length (m)	Map interval top (mbsf)	Map interval bottom (mbsf)	Map type
170	1042	A	1	R	48.7	57.8	9.1	1	0.37	0.37	48.7	49.07	STD
170	1042	A	1	R	48.7	57.8	9.1	2	0.73	0.73	49.07	49.8	STD
170	1042	A	1	R	48.7	57.8	9.1	3	0.15	0.15	49.8	49.95	STD
170	1042	A	2	R	96.1	105.7	9.6	1	0.82	0.82	96.1	96.92	STD
170	1042	A	2	R	96.1	105.7	9.6	2	0.69	0.69	96.92	97.61	STD
170	1042	A	2	R	96.1	105.7	9.6	3	0.14	0.14	97.61	97.75	STD
170	1042	A	3	R	153.7	163.3	9.6	1	1.5	1.5	153.7	155.2	STD
170	1042	A	3	R	153.7	163.3	9.6	2	0.4	0.4	155.2	155.6	STD
170	1042	A	3	R	153.7	163.3	9.6	3	0.55	0.55	155.6	156.15	STD
170	1042	A	3	R	153.7	163.3	9.6	4	0.15	0.15	156.15	156.3	STD

Note: STD = standard.

This is a sample of the table that appears on the volume CD-ROM.

The hole was displaced with 70 bbl of 10.5 lb/gal mud, and the drill string was pulled clear of the seafloor. Sepiolite mud sweeps of 30 bbl each were pumped at depths of 201.8, 211.3, and 220.9 mbsf. In addition, a 50-bbl Quick Sweep pill was pumped at a depth of 229.0 mbsf. Although the material was extremely viscous when pumped, it seemed to have little benefit over the standard sepiolite sweeps. A pump pressure increase of 100–150 psi was all that was noted as the material came out of the bit and into the annulus of the hole.

Some higher hydrocarbons were identified in this hole, but not in large quantities. The numbers dropped off rapidly after drilling through the fault-zone source. Hydrocarbon vacutainer analysis for Cores 170-142A-3R and 4R, above or within the fault, identified 0.8 and 0.7 vol% methane, 829 and 792 ppmv ethane, and 172 and 292 ppmv propane, respectively. Higher hydrocarbons included *i*-C_4 values of 40 and 79 ppmv, *n*-C_4 values of 5 and 4 ppmv, and *i*-C_5 values of 12 and 6 ppmv, respectively. In Core 4R only, *n*-C_5 values of 1 ppmv and *i*-C_6 values of 4 ppmv were measured. Data from Cores 5R and 7R (no data on Core 6R) below the fault zone identified 238,342 and 70,307 ppmv methane, 302 and 112 ppmv ethane, and 122 and 28 ppmv propane, respectively. Higher hydrocarbons included *i*-C_4 values of 47 and 11 ppmv, *n*-C_4 values of 2 and 1 ppmv, *i*-C_5 values of 3 and 7 ppmv, and *n*-C_5 values of 0.5 and 1 ppmv, respectively.

Hole 1042B

Because Hole 1042A again failed to reach the high-priority target, the problem was addressed more radically. It was thought that at least part of the drilling complications in the hole may be the result of inadequate annular clearance between the hole wall (nominal 9⅞-in diameter) and the drill collars/bottom-hole assembly (BHA; 8¼-in outside diameter). In fact, one of the most successful holes of the leg from a depth-achieved perspective was a hole drilled with the extended core barrel (XCB) drill bit, which is larger in size (11 7/16-in diameter). It was decided to make one last attempt at reaching a minimum depth of 325 mbsf by drilling a 12¼-in tricone drill-bit hole before reentering for coring.

The ship was offset 50 m to the southeast while the BHA was made up. The mudline was estimated at 3592.5 m, somewhat higher than Hole 1042A. The 12¼-in tricone bit drilled rapidly to a depth of 316.0 mbsf at an average rate of penetration (ROP) of 34.5 m/hr. There were no problems spudding with the drilling jars and correspondingly longer BHA (one extra stand of drill collars). There were no hole problems experienced during the drilling. With the bit on bottom at 316.0 mbsf, all parameters were normal. There was no evidence of overpressure, and drilling torque was smooth and constant.

A wiper trip identified tight hole from 3830.0 m (237.5 mbsf) to 3797.0 m (204.5 mbsf). Overpulls of 30 kilo-pounds (kips) were initially seen, but were reduced to normal after working the pipe through the affected area. Sepiolite mud sweeps of 30 bbl each were circulated at depths of 90.6, 119.5, 148.2, 177.1, 205.9, and 316.0 mbsf, while drilling the 12¼-in hole. After the wiper trip, the hole was displaced with 180 bbl of sepiolite drilling fluid, and the pipe was tripped back to within 100 m of the surface. The hole was again tight through the area of 237.5–204.5 mbsf, with 30 kips of overpull required.

A free-fall funnel (FFF) was made up and deployed, followed by the subsea TV camera (VIT frame). The bit was observed with the TV as it was pulled clear of the FFF and seafloor. The drill string was tripped back to the surface while recovering the subsea TV. The drill string was tripped back to the seafloor with an RCB BHA, and the drilling line was slipped and cut before attempting reentry. The search for the FFF and subsequent vessel maneuvering took 2 hr. The pipe was run in hole (RIH), without picking up the top drive, until encountering an obstruction at 151.5 mbsf. Drag was 10–15 kips, so the pipe was pulled back to a depth of 128.0 mbsf, and the top drive was picked up at that point. The subsequent trip required heavy reaming all the way to bottom. Initially there were two circulating pumps online at 75 strokes per min (spm) each. Eventually this was cut back to a single pump at 75 spm to reduce the back pressure and hydraulic pump effect resulting from the very tight formation. The rate of progress increased, torque was reduced, and hole problems declined with the use of a single circulating pump.

Once on bottom, RCB coring commenced and continued to a depth of 90.7 mbsf through alternating green mudstone and brecciated sandstone cemented with carbonates. A second wireline run was required to recover Core 170-1042B-4R when the overshot shear pin failed. Core 7R was recovered with an empty liner, so the chisel-type bit deplugger was deployed. After recovering the deplugger, a 30-bbl sepiolite mud sweep was pumped. Pump pressures increased by 400 psi when the pill came out of the bit. This was accompanied by elevated torque as well. Hole conditions remained acceptable for the cutting of Core 8R; however, the consensus of opinion was to stop coring at that point before hole conditions deteriorated. Core recovery was a poor 11.9% for the eight cores recovered, because coring parameters had to be set to optimize hole stability.

The hole was displaced with 85 bbl of 10.5 lb/gal mud, the top drive was set back, and the pipe was recovered back to the surface. The ship began DP offsetting to Site 1043 while the pipe trip continued.

No water samples or formation temperature measurements were taken in this hole, and no significant hydrocarbons were detected.

Operations at Site 1043

Before completing operations at Site 1042 with LWD, Site 1043 was cored and logged (see “Operations” section, “Site 1043” chapter, this volume). The vessel then returned to Site 1042.

Hole 1042C

LWD Hole 1042C was the last hole of Leg 170. As before, the jars were pressure tested (low 500 psi and high 3,000 psi) before making up the LWD BHA and tricone drill bit. This time the compensated density neutron (CDN) tool was left out of the BHA. Based on the previously cored holes, it was felt that without the stabilizer associated with the CDN tool, the potential for penetrating below the target reflector at this site was far greater. The compensated dual resistivity (CDR) tool was made up as part of a standard BHA, including the McCullough mechanical drilling jars. As before, it was considered safe to run the jars, because the firm bottom was likely to be drillable in a short period of time using the tricone bit. In addition, the sea state remained calm. The drill string was tripped to the seafloor, filling the pipe every 30 stands.

Hole 1042C was spudded and drilling continued at a target ROP of 35 m/hr to a depth of 35.0 mbsf, where the target ROP was decreased to 25 m/hr. Drilling continued without incident to a depth of 257 mbsf, where pump pressure was elevated by 150 psi, and some drill string torque was noted. The hole was swept with 30 bbl of sepiolite mud, and the drilling parameters returned to normal. Drilling continued to a total depth of 297.6 mbsf. A steady increase in drilling torque, coupled with persistent high pump pressure, was noted. Another 30-bbl sweep with sepiolite mud did not improve the hole condition. Because drilling was within 2.5 hr of being halted because of time constraints, it was decided to halt further LWD operations at this point. The hole was displaced with 48 bbl of 10.5 lb/gal mud. The drill string was then pulled clear of the mudline. The rig floor was secured, thrusters raised, and the vessel got underway for Balboa, Panama at 2200 hr, 14 December 1996, ending Hole 1042C.

LITHOSTRATIGRAPHY AND STRUCTURES

Description of Lithostratigraphic Units

The cores recovered at Site 1042 include two sedimentologic units (Fig. 1; Table 3). Core recovery was low (0%–27%). Coring intervals of Hole 1042A are from 48.7 to 57.8 mbsf (Core 170-1042A-1R), 96.1 to 105.7 mbsf (Core 170-1042A-2R), 153.7 to 163.3 mbsf (Core 170-1042A-3R) and from 201.7 to the bottom of Hole 1042A at 240.1 mbsf (Cores 1042A-4R through 7R). Depths and thicknesses of the units are defined based on these recovered intervals, and do not represent a continuous lithostratigraphy.

Unit 1 consists of silty claystone with minor limestone. Subunit 1B is distinguished from Subunit 1A by its minor limestone interbeds (Table 3). Subunit 1B* is lithologically identical to Subunit 1B except it contains limestone clasts rather than interbeds and was cored only in Hole 1042B below Unit 2.

Unit 2 consists of sandstone and sandstone breccia (Table 4) and is divided into Subunit 2A, in which the breccia contains angular clasts of sandstone, and Subunit 2B, in which the breccia contains angular clasts of a wide variety of lithologies in addition to sandstone (including doleritic basalt, radiolarian chert, sandstone, siltstone, and claystone).

Description of Lithologic Units

Unit 1: Silty Claystone

Interval: 170-1042A-1R-1, 0 cm, to 7R-2, 95 cm
Thickness: >154.3 m
Depth: 48.7–240.1 mbsf
Age: middle Miocene–?late Pleistocene

Table 3. Site 1042 lithostratigraphic units.

Unit	Subunit	Intervals	Thickness (m)	Depth (mbsf)	Age
1: silty claystone (48.7-240.1 mbsf)	1A: olive green silty claystone	1042A-1R-1, 0 cm, to 3R-CC, 11 cm	>114.6	48.7-163.3(?)	late Miocene to ? late Pleistocene
	1B: dark olive green silty claystone with beds of light yellowish gray limestone	1042A-4R-1, 0 cm, to 7R-2, 95 cm	>38.4	201.7-240.1(?)	middle to late Miocene?
2: breccia (316.0-353.6 mbsf)	2A: light gray carbonate cemented sandstone and sandstone breccia	1042B-1R-1, 0 cm, to 4R-1, 20 cm	>26.9	316.0-342.9(?)	early to middle Miocene?
	2B: green to grayish green breccia with clasts of doleritic basalt and chert	1042B-4R-1, 20 cm, to 5R-3, 19 cm	10.8	342.9-353.7	early to middle Miocene?
1*: silty claystone (353.6-390.8 mbsf)	1B*: dark olive green silty claystone with clasts of light yellowish gray limestone	1042B-5R-3, 19 cm, to 8R-CC, 10 cm	>37.1	353.7-390.8(?)	early/middle to late Miocene?

Table 4. Site 1042 lithologic summary.

Core	Major lithology	Color	Fossils	Diagenesis	Minor lithology	A/C/T
170-1042A-						
1R	Silty claystone Clayey ash with diatoms	Olive gray-green Med. green gray	T: rads, spicules C-: diatoms T: spicules	Si dissolution Framboids	None	
2R	Silty claystone	Dark olive green	T: forams, fish parts, pollen	Framboids, dolomite, zeolites (Phillipsite)	None	
3R	Claystone with nannofossils	Olive green	C: nannos T: diatoms, spicules, fish, forams, pollen/spores	Framboids, dolomite	Dark greenish gray claystone	C
4R	Clayey siltstone with feldspar	Olive green	C: diatoms T: rads, nannos, sponge spicules	Framboids	Lt. gray limestone	T
5R	Claystone Limestone	Dark gray green Lt. gray green	C-: diatoms; T: rads, spicules	Framboids Si diagenesis	None	

Notes: A = abundant, C+ = very common, C = common, C- = somewhat common, and T = trace. Rads = radiolarians, forams = foraminifers, nannos = nannofossils, framboids = pyrite framboids, sponges = sponge spicules, and fish = fish bones/parts.

This is a sample of the table that appears on the volume CD-ROM.

Subunit 1A: Silty Claystone

Interval: 170-1042A-1R-1, 0 cm, to 3R-CC, 11 cm
Thickness: >114.6 m
Depth: 48.7–163.3 mbsf
Age: late Miocene–?late Pleistocene

Subunit 1B: Silty Claystone and Limestone

Interval: 170-1042A-4R-1, 0 cm, to 7R-2, 95 cm
Thickness: >38.4 m
Depth: 201.7–240.1 mbsf
Age: middle–late Miocene?

Subunit 1B: Silty Claystone and Limestone*

Interval: 170-1042B-5R-3, 19 cm, to 8R-CC, 10 cm
Thickness: >37.1 m
Depth: 353.7–390.8 mbsf
Age: early/middle–late Miocene

The upper lithologic unit consists primarily of homogeneous olive green to dark olive green silty claystone to siltstone; it is divided into Subunits 1A and 1B. Silty claystones of Subunit 1A typically are dominated by abundant clay-sized grains, associated with quartz, plagioclase feldspar, and volcanic glass (Table 5). Microfossils are generally rare, with diatoms, radiolarians, sponge spicules, and fish remains present in common to trace amounts (Tables 4, 5). Volcanic glass is ubiquitous as a minor component of the sand- and silt-sized fraction. The lower part of Subunit 1A is characterized by trace amounts of nannofossils throughout Core 170-1042A-3R. All cores of this subunit were extensively disturbed by drilling, as well as by varying amounts of tectonic deformation, which may have obliterated most macroscopic sedimentary structures present. However, some intact intervals of core exhibit rare ash layers, bioturbation, and sedimentary structures. An ash layer at interval 170-1042A-1R-2, 40–70 cm (49.6–49.9 mbsf) is composed predominantly of clear, unaltered to weakly altered volcanic glass, pumice, quartz, traces of feldspar, and clay. It is mixed with diatomaceous claystone, suggesting partial reworking of the sediment by bioturbation. Burrow traces observed in a few intervals (e.g., interval 170-1042A-2R-2, 45–62 cm) also indicate bioturbation. A small fold was encountered in interval 170-1042A-3R, 59–66 cm (Fig. 5). This structure may be interpreted as a syn-sedimentary slump fold, which would indicate submarine mass transport; however, it is unclear whether the folding is natural or the product of the drilling disturbance that affects all cores of Site 1042.

In Subunits 1B and 1B*, silty claystone is dominant (Table 3), interbedded with minor layers or concretions of micritic limestone and layers of matrix-supported sedimentary breccia. The breccia consists of angular to subrounded clasts of claystone, siltstone, glauconitic sandstone, and light greenish gray limestone. Clasts are up to 2 cm in diameter (Fig. 6). Thin layers of glauconitic sandstone were encountered in Cores 170-1042A-4R and 7R. At intervals 170-1042A-4R-1, 5–12 cm, and 170-1042A-4R-2, 41–47 cm, layers of dark olive green siltstone are enriched in foraminifers. A 40-cm-thick layer of yellowish gray, strongly lithified micritic limestone was recovered in interval 170-1042A-5R-1, 40 cm, to 5R-2, 10 cm (211.7–212.1 mbsf). In interval 170-1042A-7R-2, 61–69 cm, a sandy micritic limestone was recovered (Fig. 7). In Sample 170-1042B-8R-2, 40 cm, a small micritic limestone concretion occurs within the silty claystone. Below Core 170-1042A-5R, clasts of micritic limestone are common within fill material at the top of the recovered cores. The micritic limestone contains up to 10% fine sand and a trace of medium to coarse sand-sized grains of quartz and plagioclase feldspar, as well as trace amounts of volcanic glass, rock fragments, and glauconite. Foraminifers are common and well preserved; remains of diatoms, radiolarians, and sponge spicules occur in trace amounts. The matrix is composed of relatively coarse-grained micrite as well as clay minerals, suggesting diagenetic carbonate cementation of a silty claystone.

Diagenetic pyrite framboids form a minor to trace component throughout Unit 1 and are also present in the micritic limestone. Trace amounts of fine silt-sized dolomite rhombs were also noted in smear slides from Cores 170-1042A-2R through 6R (96.1–230.5 mbsf; Table 5).

Unit 2: Breccia

Interval: 170-1042B-1R-1, 0 cm, to 5R-3, 19 cm
Thickness: >37.6 m
Depth: 316–353.6 mbsf
Age: early–middle Miocene?

Subunit 2A: Light Gray Carbonate-Cemented Sandstone and Sandstone Breccia

Interval: 170-1042B-1R-1, 0 cm, to 4R-1, 20 cm
Thickness: >26.9 m
Depth: 316.0–342.9 mbsf
Age: early–middle Miocene?

Subunit 2B: Green to Grayish Green Breccia with Clasts of Doleritic Basalt, Chert, and Sandstone

Interval: 170-1042B-4R-1, 20 cm, to 5R-3, 19 cm
Thickness: 10.8 m
Depth: 342.9–353.6 mbsf
Age: early–middle Miocene?

Unit 2 consists of thick lithified layers of breccia. The total thickness of this unit is 37.6 m (interval 170-1042B-1R through 5R-3, 19 cm; 316.0–353.6 mbsf). However, the top of the breccia unit was not cored. In intervals 170-1042B-1R-1, 0–11 cm, 170-1042B-2R-1, 0–17 cm, 170-1042B-3R-1, 0–11 cm, 170-1042B-4R-1, 0–22 cm, and 170-1042B-5R-1, 0–30 cm, pebbles of silty claystone and micritic limestone represent hole fill material from layers above, and, therefore, they are not considered part of Unit 2.

The breccia of Subunit 2A consists of sandstone fragments from granule size to clasts as large as >10 cm (Fig. 8). Some of the sandstone clasts are layered at a millimeter- to centimeter-scale (Figs. 8, 9). Based on thin-section observations, the sandstone is composed of terrigenous clastic material, mostly plagioclase feldspar with minor amounts of quartz, pyroxene, and/or amphibole. Rock fragments include sandstone, recrystallized chert, and large round pumice fragments (>1 cm). Glauconite is present in trace amounts. Both the sandstone clasts and the sandy matrix of the breccia are carbonate cemented and commonly contain well-preserved foraminifers.

Structures within the breccia of Subunit 2A include numerous healed fractures (Figs. 8, 9) and filled fractures or veins (Fig. 10). The healed fractures range from diffuse gaps across which angular fragments can be fitted together (e.g., interval 170-1042B-1R-1, 92–97 cm, left side of Fig. 8) to sharp thin zones bounding angular to subrounded fragments of sandstone or sandstone breccia (e.g., interval 170-1042B-1R-1, 84–97 cm, right side of Fig. 8). In addition, at least three different generations of veins may be distinguished (Fig. 10A). The first generation is composed of thin (<1 mm) calcite veins randomly oriented to form a pervasive network. These are displaced by thicker veins (2–3 mm) of the second generation composed of fibrous calcite. The third vein generation, displacing both first and second generation veins, is much thicker (>1 cm) and locally has 2- to 5-mm-wide voids lined with euhedral calcite crystals (Fig. 10B).

Subunit 2B is defined by a breccia with clasts mainly of doleritic basalt and chert, plus sandstone, siltstone, and claystone. Chert clasts are up to 2 cm in diameter; basaltic clasts are up to 5 cm in diameter. This breccia is not graded (Fig. 11), but contains fragments of laminated sandstone and siltstone, some with multiple generations of calcite veins. Fragments of micritic limestone, slightly chloritized mafic rocks (according to X-ray diffraction [XRD] data, see “Geochemistry” section, this chapter), plagioclase feldspar, quartz, glauconite,

Table 5. Site 1042 smear-slide descriptions.

Sample number							Depth	Imp.		Size			Composition															Fossils								Sediment or rock name	Comments
Leg	Site	Hole	Core	Type	Section	Interval (cm)	mbsf	Major lithology	Minor lithology	Med.-coarse sand	Fine sand	Silt size	Clay size	Quartz	Feldspar	Clay	Rock fragments	Volcanic Glass	Amphibole	Glauconite	Phosphate	Dolomite	Carbonate	Micrite	Opaque	Framboid	Nannofossils	Foraminifers	Diatoms	Radiolarians	Silicoflagellates	Sponge spicules	Fish remains	Peloids/pellets	Other		
170	1042	A	1	R	1	2	48.72		X			A	C	C-	T	C		A		T						C-			C-			T				Vitric ash mixed with diatomaceous claystone	
170	1042	A	1	R	CC	3	49.83	X				C	A	T	T	A	T	T				T								T		T				Olive green claystone	
170	1042	A	2	R	2	22	97.14	X			T	C	A	T	C	A	C	C-	T	T		T+	T	T	T	T		T					T		T	Dark olive green silty claystone	Other = pyroxene? (T), pollen/spores (T), zeolites (Phillipsite, T). Rock fragments are pumice, polycrystalline quartz (volcanic).
170	1042	A	3	R	3	16	155.76		X		T	C-	A	T	T+	A	T	C				T+	T	T		T+	T	T			T	T		T	Dark greenish gray claystone	Other = pollen/spores
170	1042	A	3	R	3	33	155.93	X				T	A	T	T	A		T				T	T	T	T	T	C		T			T	T			Olive green claystone with nannofossils	
170	1042	A	4	R	1	99	202.69		X			C+	A					T			T		C+	A		T			T			T				Light gray limestone	
170	1042	A	4	R	2	56	203.52	X			T	C+	C	C-	C+	C		C-		C-		T	C-			C-	T		C-	T		T				Clayey siltstone	
170	1042	A	5	R	1	51	211.81	X				A	A					T			T		A	A	T	T										Light greenish gray limestone	
170	1042	A	5	R	2	63	212.63	X				C-	A	C-	T	A		T			T					C			C-	T						Dark gray green claystone	
170	1042	A	6	R	2	82	221.92				T	C	A	T	C	A	C	C		T		T	T			T	T		C			T	T			Dark greenish gray silty claystone	

Notes: Imp. = importance. A = abundant, C+ = very common, C = common, C- = somewhat common, T+ = strong traces, T = trace, and blank box = not observed.

This is a sample of the table that appears on the volume CD-ROM.

Figure 5. Sketch of a small, possibly syn-sedimentary, slump fold (interval 170-1042A-3R-1, 59–66 cm).

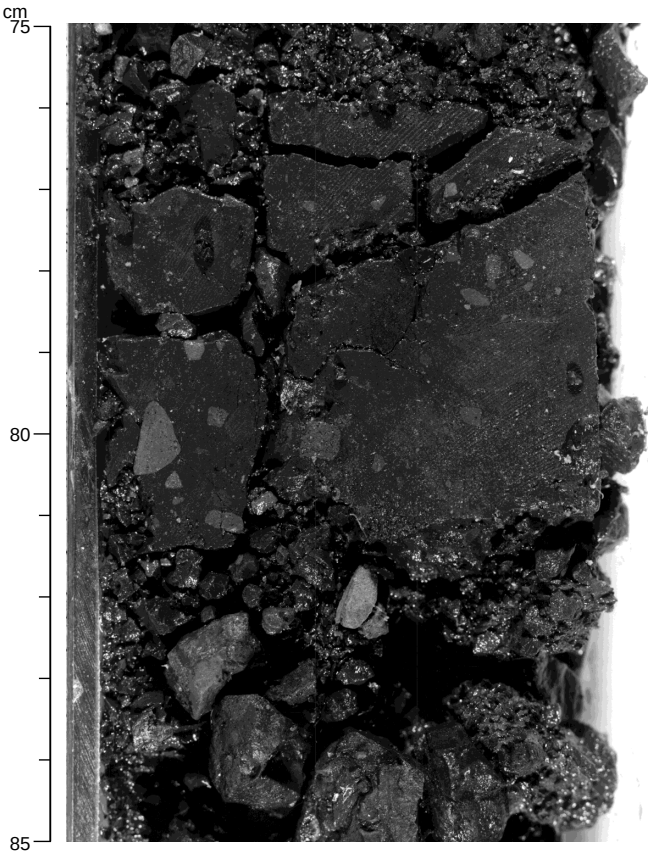

Figure 6. Matrix-supported sedimentary breccia at the base of Subunit 1B (interval 170-1042A-7R-2, 75–85 cm).

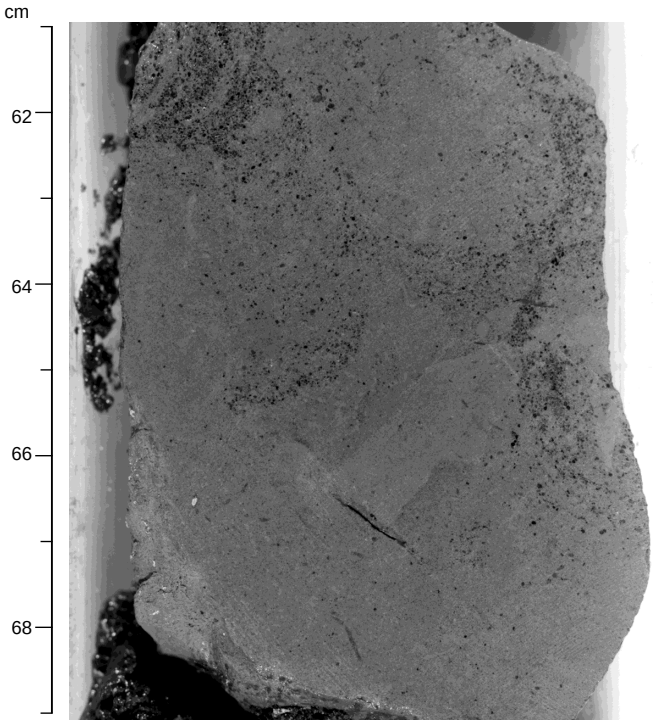

Figure 7. Micritic limestone with terrigenous sand of Subunit 1B (interval 170-1042A-7R-2, 61–69 cm).

and olivine occur in trace amounts. The matrix is composed mainly of micritic carbonate. The chert is recrystallized, obscuring its original nature. The doleritic basalt consists of plagioclase feldspar and olivine phenocrysts in an aphanitic groundmass of chlorite and clay minerals. The mineral composition, the estimated mineral proportions, and the shipboard X-ray fluorescence (XRF) data for the doleritic basalt clasts are different from the gabbro intrusions encountered at Sites 1039 and 1040. The XRF data indicate a tholeiitic basalt composition with depleted immobile and incompatible trace elements and enriched Ba, suggesting an arc affinity (see “Geochemistry” section).

At least two generations of calcite-filled veins cross-cut individual clasts, but terminate at clast boundaries (Fig. 11); therefore they predate the brecciation. At least two additional vein sets probably post-date the brecciation. The first of these is characterized by thin calcite-filled veins (<1 mm) arranged in parallel swarms. The second generation of post-breccia veins consists of up to 5-mm-thick veins that contain multiple generations of calcite and zeolite.

Structures

In addition to the veins described above, the cores at Site 1042 exhibit a few horizons of brittle and plastic deformation. Bedding attitudes are poorly defined because of the widely spaced coring and poor recovery. The few bedding surfaces observed generally have a dip of 35°–45°. Structural observations at Site 1042 indicate that the 390-m-thick section of sediments can be divided into two tectonic units. The most important structural feature is a shear zone at 353.7 mbsf (in Core 170-1042B-5R). Below Unit 2B, part of Unit 1B appears to be repeated. An age inversion from early Miocene in Unit 2B in the hanging wall to late Miocene in Subunit 1B* in the footwall (see “Biostratigraphy and Magnetostratigraphy” section, this chapter) supports the interpretation of this feature as a thrust fault. This 40-cm-wide shear zone (interval 170-1042B-5R-1, 82 cm, to 5R-2, 10 cm), contains plastically deformed material and includes rocks apparently derived from the breccia of Unit 2B (Fig. 12). It is interpret-

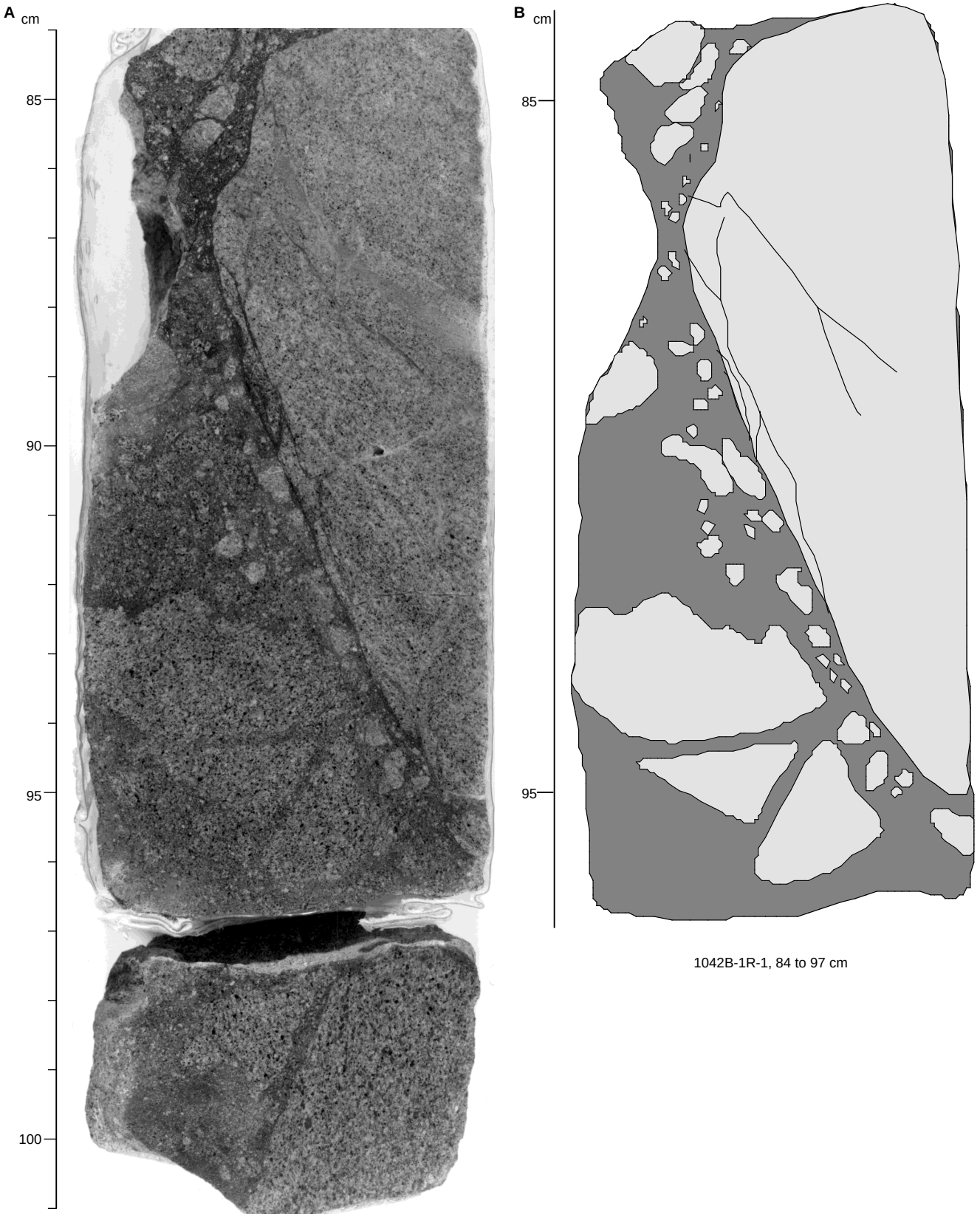

Figure 8. **A.** Carbonate-cemented sandstone breccia of Subunit 2A (interval 170-1042B-1R-1, 84–101 cm). **B.** Sketch of this breccia (interval 170-1042B-1R-1, 84–97 cm).

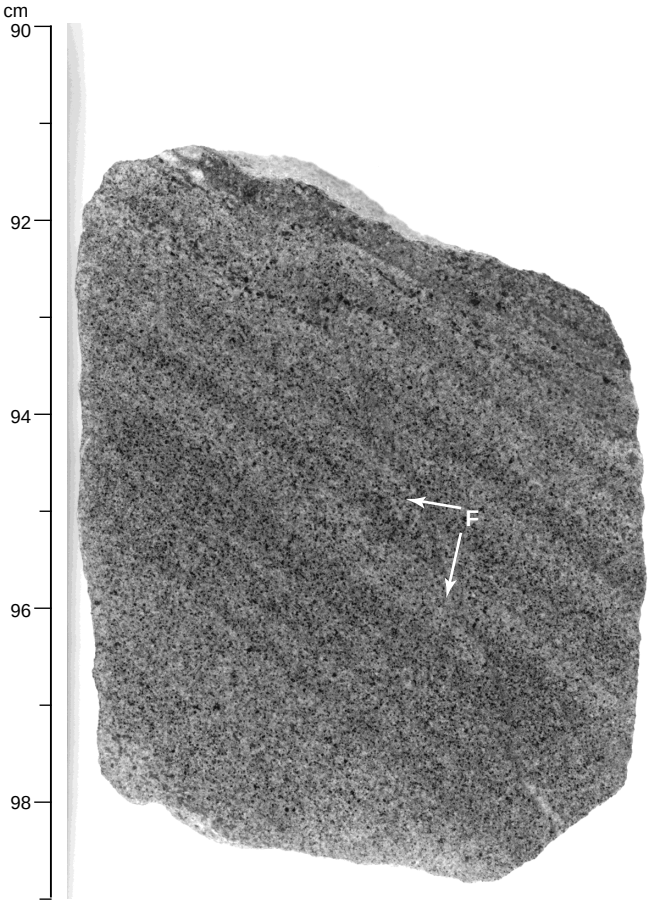

Figure 9. Carbonate-cemented sandstone with typical millimeter- to centimeter-scale layering. A small-offset fracture ("F") crosses the sample diagonally (Subunit 2A, interval 170-1042B-1R-2, 90–99 cm).

ed to have formed at the base of the thrust sheet. Part of the shear zone may have been lost because of incomplete recovery.

Below the thrust fault, the silty claystone of Subunit 1B is highly fractured with the development of scaly fabric marked by extremely polished lenticular rock pieces (entire Core 170-1042B-6R). This scaly fabric is limited to Cores 170-1042B-5R and 6R.

Discussion and Summary

Unit 1 is composed of massive silty claystone to siltstone, with a few interbedded ash layers and thin glauconitic sandstone beds. The predominantly fine-grained terrigenous components and the lack of clear grading or bedding are consistent with a deepwater hemipelagic origin on the lower continental slope. Sedimentary breccias and rare, small slump folds in the lower part of Unit 1 suggest that downslope mass transport processes (i.e., gravity flow and slumping) have mixed and reworked at least part of Unit 1. Both downslope transport and bioturbation may have contributed to the mixing and disruption of ash and sand layers. Micritic limestone in the lower part of Unit 1 is probably diagenetically cemented silty claystone.

Unit 2 is composed of carbonate-cemented sandstone and sandstone breccia, and a breccia of sedimentary and igneous rocks. The carbonate-cemented sandstone appears to have first been broken and mixed with a loose sand matrix, and then the mixture was cemented together. The breaking may have been tectonic, because some of the pieces fit back together like a fault breccia. However, clasts of the chert and basalt breccia do not fit back together. This breccia may have been transported by submarine mass wasting. Rocks similar to both the chert and the doleritic basalt, as well as to the minor components of the breccia of Subunit 2B, are exposed in the Nicoya ophiolite complex on the nearby Nicoya Peninsula, Costa Rica (Kuijpers, 1980; Berrangé and Thorpe, 1988). These components could have been derived from the Nicoya complex.

None of the cored material at Site 1042 in the apron is lithologically similar to the reference section at Site 1039. The depth to the Unit 2 breccia coincides with the prominent top-of-prism reflection visible in the seismic-reflection profile (see "Background and Objectives" section, this chapter). This breccia appears to have been thrust faulted over the silty claystones of Subunit 1B*. Its strong lithification by carbonate cement may account for that reflection.

BIOSTRATIGRAPHY AND MAGNETOSTRATIGRAPHY

Biostratigraphy

Calcareous Nannofossils

Hole 1042A

The results of the biostratigraphic analysis of calcareous nannofossils from Hole 1042A must be taken in context with the events surrounding the coring effort. Hole 1042A was spot cored in ~50-m increments to a depth of 231.65 mbsf. Seven rotary cores were recovered. Several wiper trips and hole sweeps were conducted while attempting to recover Cores 170-1042A-6R and 7R; these cores may exhibit considerable downhole contamination. Because of poor core recovery and the large ~50-m sampling intervals, a detailed nannofossil biostratigraphy could not be done. Nevertheless, a calcareous nannofossil range distribution is presented in Table 6 and Figure 13. Cores 170-1042A-1R and 2R could not be assigned to a zone. Sample 170-1042A-3R-CC can only be determined to be older than 3.75 Ma (last occurrence [LO] datum of *Reticulofenestra pseudoumbilica*). Core-catcher samples from Cores 170-1042A-4R through 6R could not be zoned. Core 170-1042A-7R contains an assemblage of nannofossils that are characteristic of middle Miocene Zone NN5.

Hole 1042B

Seven sediment cores were recovered from Hole 1042B with bottom depths of 333.26–383.47 mbsf. Table 6 presents the range and distribution of calcareous nannofossils observed in cores from this hole. The calcareous nannofossil assemblage in Sample 170-1042B-3R-CC is characteristic of early Miocene Zone NN4. The assemblages of nannofossils in Samples 170-1042B-5R-CC and 6R-CC contain *Discoaster berggreni,* and very few earlier Miocene species. This would place these two assemblages in the earliest Pliocene–late Miocene NN11 Zone, considerably younger than the overlying interval. This inversion could be explained by faulting and tectonic activity or by downhole contamination. Sample 170-1042B-8R-CC is placed in the early middle Miocene NN5 Zone, based on the occurrence of *S. heteromorphus* and the absence of *H. ampliaperta.*

Diatoms

Hole 1042A

Diatoms from cores recovered at Site 1042A are absent to common and show poor preservation, which prevents detailed diatom biozonation of the cores (Table 7; Fig. 13). Rare and poorly preserved diatoms in Samples 170-1042A-1R-CC (49.93 mbsf) through 4R-CC (203.92 mbsf) did not yield age-significant taxa. Sample 170-1042A-5R-CC has common but poorly preserved diatoms and contains *Nitzschia reinholdii, Thalassiosira convexa* var. *aspinosa,* and *Nitzschia miocenica* (LO 6.06 Ma), suggesting an age of late Miocene, correlating to *Thalassiosira convexa* Subzone B. Sample 170-1042A-6R-CC also has *N. miocenica* and *N. reinholdii,* in addition to

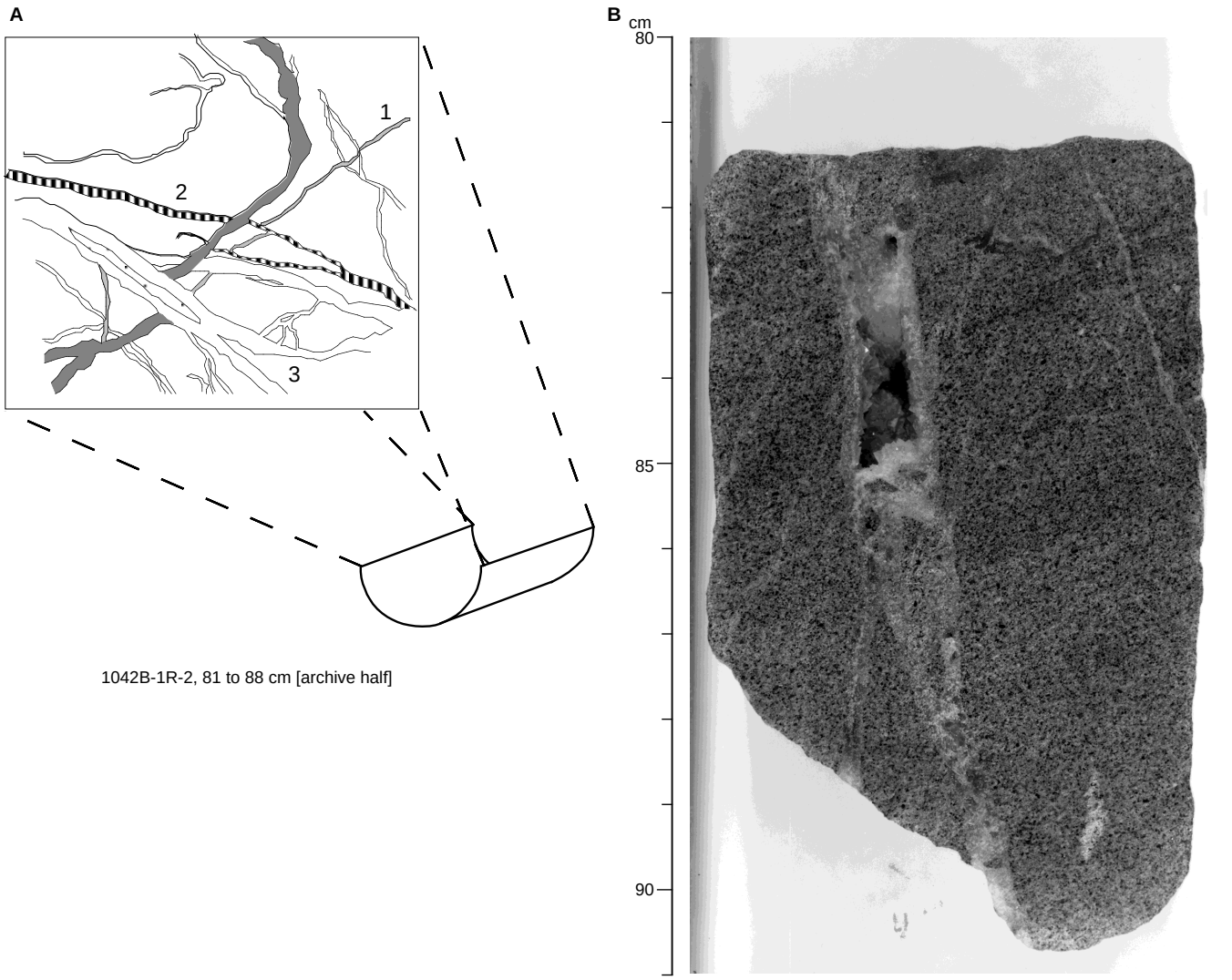

Figure 10. **A.** Sketch of at least three vein generations visible around the outside of the half-core in B. **B.** Calcite vein (third generation) enclosing a cavity lined with euhedral calcite crystals in sandstone of Subunit 2A (interval 170-1042B-1R-2, 80–91 cm).

Thalassiosira praeconvexa, which has a LO at 6.17 Ma and is characteristic of the late Miocene. Sample 170-1042A-7R-CC has only rare diatoms that show poor preservation, and no age determination is possible.

Hole 1042B

Diatoms in Samples 170-1042B-2R-1, 14–16 cm (~325 mbsf), and 3R-CC continue to be rare in abundance and poorly preserved. However, in Sample 170-1042B-4R-1, 73–75 cm (~343 mbsf), diatoms are few and more moderately preserved and suggest an early middle Miocene age. *Denticulopsis hustedtii, Crucidenticula nicobarica, Coscinodiscus lewisianus*, and *Cestodiscus pulchellus* are characteristic of the *C. lewisianus* Zone that ranges between 12.86 and 14.03 Ma. Unfortunately, diatoms recovered from Samples 170-1042B-5R-CC through 6R-CC (Table 7) are only rare and very poorly preserved, preventing an age assignment for this part of the hole.

Planktonic Foraminifers

Planktonic foraminifers are rare to barren in all core-catcher samples of Holes 1042A and 1042B (Table 8). Some zonal intervals were identified on the basis of a few diagnostic species.

Hole 1042A

Seven cores were recovered from Hole 1042A. Planktonic foraminifers from Hole 1042A are rare to absent (Table 8). When present, their preservation is moderate to poor. Sample 170-1042A-1R-CC is assigned to the Pleistocene Zone N22 based on the co-occurrence of *Globorotalia bermudezi* and *Neogloboquadrina humerosa.* The age of Samples 170-1042A-2R-CC and 3R-CC is between 3.95 and 6.0 Ma, based on occurrence of sinistrally coiled *Pulleniatina* spp. and *Globorotalia margaritae.* The age of Sample 170-1042A-7R-CC is younger than 8.1 Ma, based on presence of *Globorotalia juanai.* Samples 170-1042A-5R-CC and 6R-CC are barren of planktonic foraminifers.

Hole 1042B

Eight cores were recovered from Hole 1042B. Planktonic foraminifers from Hole 1042B are rare to absent except in Sample 170-1042B-3R-CC, which yielded a few planktonic foraminifers, but preservation is poor (Table 8). Samples from this hole that were analyzed for planktonic foraminifers are Samples 170-1042B-3R-CC, 5R-CC, 6R-CC, and 8R-CC.

Sample 170-1042B-3R-CC was assigned to Zone N8 (earliest middle Miocene), based on the occurrence of *Globigerinoides sica-*

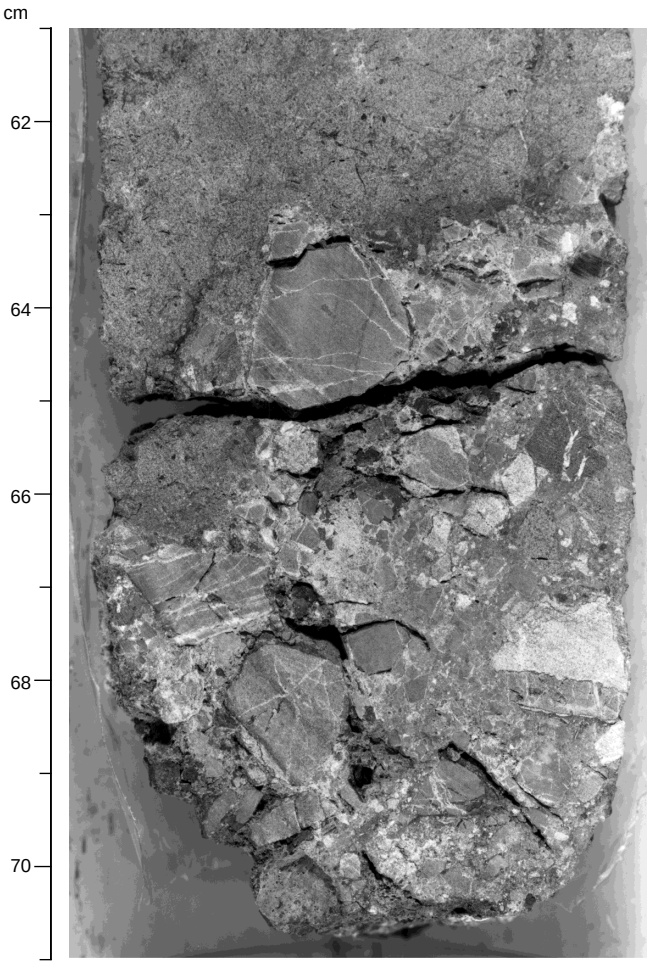

Figure 11. Breccia with angular clasts of doleritic basalt, chert, and laminated siltstone and sandstone (some with calcite veins; Subunit 2B, interval 170-1042B-5R-1, 61–71 cm).

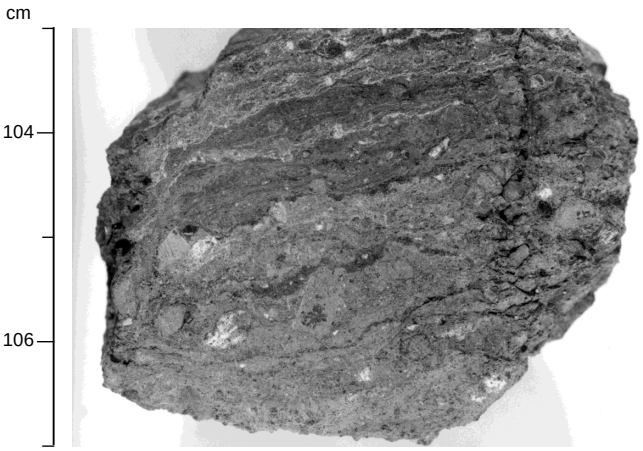

Figure 12. Part of shear zone at the base of Subunit 2B (interval 170-1042B-5R-1, 103–107 cm).

nus and the absence of *Orbulina* spp. In Sample 170-1042B-5R-CC, middle Miocene to early Miocene planktonic foraminifers are mixed. Sample 170-1042B-6R-CC includes *Globorotalia conoidea* and *Neogloboquadrina acostaensis* of the late Miocene. Sample 170-1042B-8R-CC is assigned to Zone N12 (late middle Miocene) based on the co-occurrence of *Globorotalia foshi lobata* and *Globorotalia praemenardii.*

Paleomagnetism

Because of the spot coring at Hole 1042A and the poor recovery and complex lithology of Hole 1042B, little interpretation can be made of the magnetostratigraphy at this site. Pass-through measurements of split cores after 20-mT demagnetization of sediments from Hole 1042A show both normal and reversed polarity (Fig. 14). Results from Hole 1042B also show both normal and reversed polarities. Of note are the dual polarities and high (700–900 mA/m) remanence intensities from the intervals containing red chert fragments (Fig. 15).

GEOCHEMISTRY

Overview

The main geochemical scientific objectives at this site, located ~8 km southwest of Site 1041, are the same as for Site 1041 (see "Geochemistry" section, "Site 1041" chapter, this volume). Cores were taken only every 50 m to a depth of 200 mbsf, and continuous coring resumed below this depth; however, recovery was poor. The concentration depth profiles, therefore, consist of only a few data points sparsely distributed throughout the depth drilled. All of the pore-fluid samples analyzed are from beneath the sulfate-reaction zone. Methane concentrations are already high in the shallowest first sample analyzed, at ~50 mbsf. The section drilled lies within the stability field of methane hydrate, and mild gas escape was observed in the few sediment samples obtained from ~100 to 230 mbsf. Most likely the hydrate is responsible for at least some of the C_l freshening also encountered at this site. An abrupt increase in the content of C_1 through C_3 and traces of higher hydrocarbons through C_6 were observed between 150 and 200 mbsf, where a major fault was intersected (Tables 9 and 10), suggesting formation at ≥100°C.

A change in the pore-fluid chemistry occurs at ~100 mbsf. Below ~100 mbsf, including across the fault zone to ~230 mbsf, the pore-fluid chemistry has characteristics similar to the fluids observed at Site 1041 beneath the conduit at 280–300 mbsf and at Site 1040 beneath the conduit at ~180 mbsf. For example, Ca concentrations are elevated and the Cl concentrations and Na/Cl values are lower than those in seawater. The physical properties also change at ~100 mbsf, with bulk densities increasing from 1.6 to 1.8 g/cm^3 and porosities decreasing by ~14%–52%, as they also do at the corresponding depth intervals cited above at Sites 1041 and 1040 (see "Physical Properties" section, this chapter). Over the 100-m interval of no recovery between 230 and 330 mbsf, the changes in the chemical nature of the pore fluids are conspicuous: the salinity, Cl, K, and Mg concentrations decrease, as do the Na/Cl values, and the Ca concentrations increase dramatically to ~103 mM. Such highly altered pore fluids, especially the very high Ca concentration, could evolve by extensive low to moderate temperature reactions between seawater (pore fluid) and volcanic sediments in a virtually closed system, as observed, for example, in the Izu-Bonin forearc sedimentary basin at Site 793 (Taylor, Fujioka, et al., 1990) or in an evaporative system. In both scenarios, the salinity and Cl concentration will increase and exceed seawater values, although this is not the case at this open-system site. Coupled reactions, including volcanogenic sediments and/or oceanic basement at moderate to elevated temperatures, are necessary to freshen the fluid and simultaneously increase its Ca concentration. Over this depth interval (230–330 mbsf) porosities

Table 6. Calcareous nannofossil range distribution chart for Holes 1042A and 1042B.

Calcareous nannofossil zone	Core, section	Depth (mbsf)	Abundance	Preservation	Small reticulofenestrids	*Calcidiscus leptoporus*	*Coccolithus miopelagicus*	*Cyclicargolithus floridanus*	*Discoaster quinqueramus*	*Helicosphaera carteri*	*Sphenolithus heteromorphus*	*Sphenolithus moriformis*	*Sphenolithus verensis*	*Discoaster brouweri*	*Discoaster variabilis*	*Helicosphaera sellii*	*Reticulofenestra pseudoumbilicus*	*Coccolithus pelagicus*	*Gephyrocapsa caribbeanica*	*Coccolithus pelagicus*	*Calcidiscus macintyrei*	*Discoaster berggrenii*	*Discoaster deflandrei*	*Helicosphaera ampliaperta*
	170-1042A-																							
?	1R-CC	49.93	F	P	F	F				R														
	2R-CC	97.73	R	P	R	R																		
>NN15	3R-CC	156.26	F	P	F	F				R		F	F	R	R	R	R							
	4R-CC	203.92	B																					
?	5R-CC	212.88	B																					
	6R-CC	223.18	R	P		R						R												
NN5	7R-CC	231.65	R	P	R	R	R		R	R	R	R	R											
	170-1042B-																							
NN4	3R-CC	333.26	A	M		A	A	A		A	A	A	C				A	R	d				C	A
	5R-CC	354.72	F	P	F					F		F	F								R	R		
NN11?	6R-CC	363.14	R	P					R			R	R							R				
NN5	8R-CC	383.47	F	P			F	F		F	F	F	A				F							

Notes: Abbreviations for abundances are as follows: A = abundant, C = common, F = few, R = rare, B = barren, d = downhole contamination. Abbreviations for preservation are as follows: G = good, M = moderate, and P = poor. For more specific definitions refer to the "Explanatory Notes" chapter (this volume).

This table also appears on the volume CD-ROM.

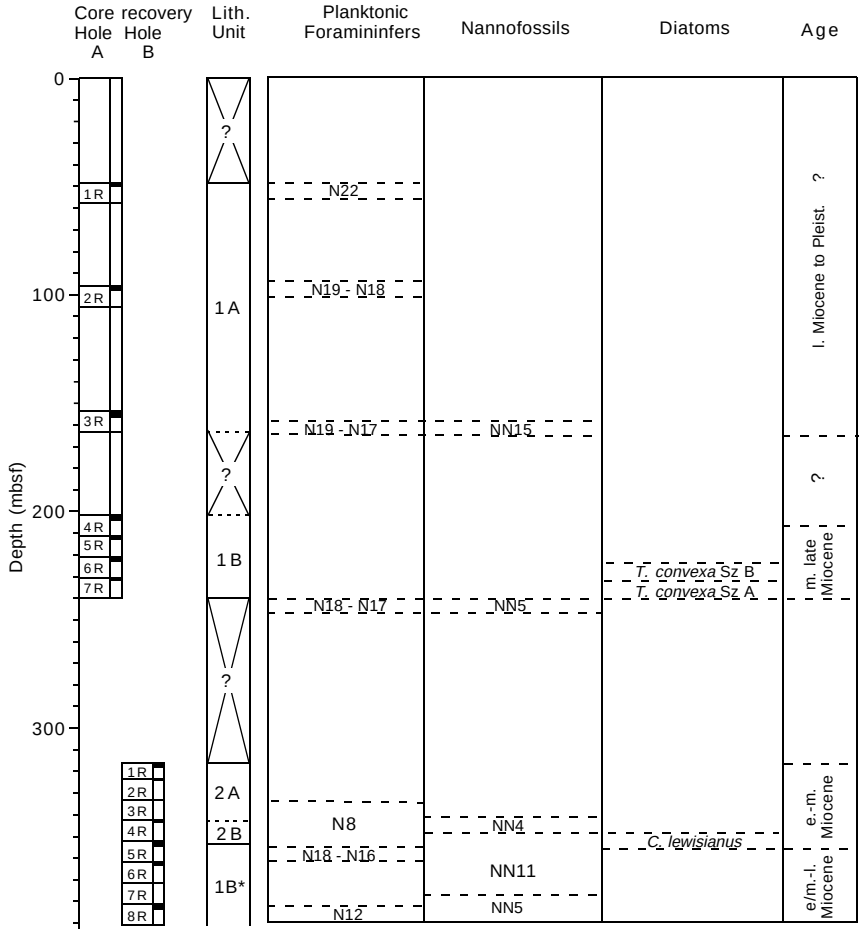

Figure 13. Correlation of the planktonic foraminifer, calcareous nannofossil, and diatom zones with Site 1042 cores and sedimentary units. Dashed lines represent uncertainty in placement of the zonal boundary.

Table 7. Diatom range distribution chart for Holes 1042A and 1042B.

Diatom zone	Core, section	Depth (mbsf)	Abundance	Preservation	*Actinoptychus senarius*	*Azpeitia nodulifer*	*Cestodiscus pulchellus*	*Coscinodiscus lewisianus*	*Coscinodiscus marginatus*	*Crucidenticula nicobarica*	*Denticulopsis hustedtii*	*Nitzschia miocenica*	*Nitzschia reinholdii*	*Rossiella paleacea*	*Thalassionema nitzschioides*	*Thalassiosira convexa* var. *aspinosa*	*Thalassiosira oestrupii*	*Thalassiosira praeconvexa*	*Thalassiothrix longissima*
	170-1042A-																		
	1R-CC	49.93	R	P											R				R
?	2R-CC	97.73	B																
	3R-CC	156.26	R	P	R										R				R
	4R-CC	203.92	R	P	R										R				R
T. convexa Sz B	5R-CC	212.88	C	P			r		R			R	R	r	F	F	R		F
T. convexa Sz A	6R-CC	223.18	F	M	R							F	R		R	R	R	F	R
	7R-CC	231.65	R	P			r								R				R
?	170-1042B-																		
	3R-CC	333.26	R	P															R
C. lewisianus	4R-1, 73-75	334.01	F	M			R	R		R	F								
	5R-CC	354.72	R	P		R			R						R				R
?	6R-CC	363.14	B																
	8R-CC	383.47	R	P					R										

Notes: Abbreviations for individual species abundances are as follows: A = abundant, C = common, F = few, R = rare, B = barren, and r = reworked. Abbreviations for preservation are as follows: G = good, M = moderate, and P = poor. For more specific definitions refer to the"Explanatory Notes" chapter (this volume). Sz = subzone.

This table also appears on the volume CD-ROM.

also decrease sharply, and in the cemented breccias of lithologic Unit 2 (see "Lithostratigraphy and Structures" section, this chapter) the porosity is down to 10%–20% (see "Physical Properties" section, this chapter).

The detrital components of the apron sediments are chemically more homogeneous than at Site 1041 and are more similar to the wedge sediments at Site 1040. Carbonate-cemented sedimentary clasts in the breccias have low trace element concentrations for all but Sr, suggesting that they are relatively clean sandstones with little heavy mineral accumulation. Basaltic clasts admixed with carbonate and chert have mafic to very mafic compositions with up to 12 wt% MgO, 549 ppmv N, and 1184 ppmv Cr. The TOC and IC contents, as well as the sulfur concentrations, however, more clearly resemble the values at Site 1041 than those at Site 1040. At the latter site, concentrations are generally somewhat lower with larger variations.

Gas Results

Methane concentrations in the headspace volumes range between 3,238 and 356,147 ppmv. The highest methane contents were measured in Section 170-1042-3R-1 (Table 9). Ethane and propane were detected in considerable quantities, with ethane concentrations from 8 ppmv (48.73 mbsf) to 444 ppmv (153.73 mbsf; Table 9). High propane contents (up to 106 ppmv at 203.23 mbsf) probably indicate an input of thermogenic gas from a deeper source.

The four vacutainer samples obtained were found to contain hydrocarbons in the C_1 (methane) to C_6 (hexane) range (Table 10). The hydrocarbon concentrations are significantly higher (up to 99.9 vol%) than those obtained by headspace technique, but they present similar gas ratios for equivalent depth intervals. In all samples analyzed, a significant amount of higher hydrocarbons were detected, which probably reflect an admixture of thermogenic gas.

Pore-Water Results

The low recovery of fluids at this site, especially below 230 mbsf, did not permit analysis for the full spectrum of geochemical parameters.

Chloride and Salinity

Chloride concentrations decrease at an average gradient of 52 mM/100 m. In the top 100 mbsf and below ~230 mbsf to the bottom of the site, the gradient is somewhat steeper, about 85 mM/100 m, whereas the concentrations decrease only slightly across the fault zone (from ~100 to 230 mbsf; Fig. 16A; Table 11). The datum point in the parenthesis at the bottom of the figure is from the last core that included a large amount of rubble; therefore, this pore fluid is not truly representative of the designated depth and is not included in the discussion. On the basis of the other geochemical data, below ~50 mbsf the low Cl fluid at this site is representative of the second deeper fluid at Site 1041. The salinity depth profile shows a parallel division into the three depth intervals (Fig. 16A). The origin of the deeper seated low-Cl fluid has been discussed in detail in the "Geochemistry" section of the "Site 1041" chapter (this volume). Thus, most of the section permeated by the upper, shallower low-Cl fluid at Site 1041 is missing at this site, a conclusion also supported by the physical properties discussed in the overview.

Sodium and Potassium

Both the Na/Cl values and the K concentrations decrease only slightly to about ~230 mbsf (Figs. 16C; 16D). This is most likely an "artifact," the result of ion-exchange reactions with ammonium and in situ release of Na and K into the pore fluids, as seen and discussed at Sites 1040 and 1041. Below 230 mbsf, the Na/Cl values and K concentrations decrease steeply, indicating that the deep-seated fluid is depleted in Na and K, as it is at Sites 1040 and 1041, suggesting a common source.

Calcium, Magnesium, and Silica

Below ~50 mbsf, Ca concentrations increase with depth. The increase is particularly steep between ~230 and 360 mbsf, where the Ca concentration gradient is ~0.6 mM/m, reaching a maximum value of 103 mM at 362 mbsf (Fig. 17A). Except for the Izu-Bonin forearc basin Sites 792 and 793 (Taylor, Fujioka, et al, 1990) and evaporite sys-

Table 8. Planktonic foraminfer range distribution chart for Holes 1042A and 1042B.

Planktonic foraminifer zone	Core, section	Depth (mbsf)	Abundance	Preservation	*Dentoglobigerina altispira*	*Globigerina falconensis*	*Globigerinatella insueta*	*Globigerinita uvula*	*Globigerinoides extremus*	*Globigerinoides immaturus*	*Globigerinoides obliquus*	*Globigerinoides ruber*	*Globigerinoides sacculifer*	*Globigerinoides sicanus*	*Globigerinoides subquadratus*	*Globigerinoides trilobus*	*Globoconella conoidea*	*Globoquadrina venezuelana*	*Globorotalia bermudezi*	*Globorotalia birnageae*	*Globorotalia fohsi lobata*	*Globorotalia juani*	*Globorotalia margaritae*	*Globorotalia menardii*	*Globorotalia merotumida*	*Globorotalia peripheroronda*	*Globorotalia siakensis*	*Neogloboquadrina acostaensis*	*Neogloboquadrina continuosa*	*Neogloboquadrina dutertrei*	*Neogloboquadrina humerosa*	*Neogloboquadrina mayeri*	*Pulleniatina obliquiloculata*	*Pulleniatina primalis*	*Sphaeroidinellopsis seminulina*	*Tenuitella clemenciae*	*Zeaglobigerina rubescens*	*Zeaglobigerina woodi*
	170-1042A-																																				
N22	1R-CC	49.93	R	M								R	R			R			R					R					R	R		R			R		
N19-N18	2R-CC	97.73	R	P					R														R	R			R			R			R	R	R		
N19-N17	3R-CC	156.26	R	P	R				R		R	R						R						R			R								R		
	4R-CC	203.92	T	P																							T									T	
	5R-CC	212.88	B																																		
	6R-CC	223.18	B																																		
N18-N17	7R-CC	231.65	R	M				R										R				R		R													
	170-1042B-																																				
N18	3R-CC	333.26	F	P	R						R		R	R	R	R		R		R				R		R		R				R					
	5R-CC	354.72	R	P	R		T				R					R		R						R	T	R	R										
N18-16	6R-CC	363.14	R	P													T										T									T	
N12	8R-CC	383.47	R	M		R				R	R							R			R											R			R		

Notes: Abbreviations for abundances are as follows: A = abundant, C = common, F = few, T = trace, R = rare, and B = barren. Abbreviations for preservations are as follows: G = good, M = moderate, and P = poor. For more specific definitions refer to the “Explanatory Notes” chapter (this volume).

This table also appears on the volume CD-ROM.

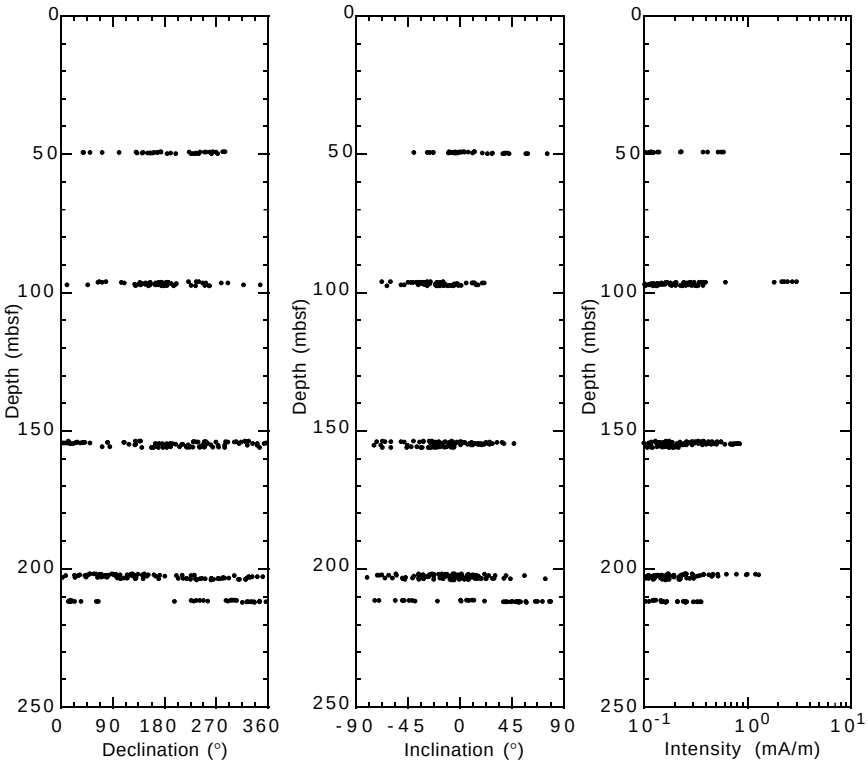

Figure 14. Pass-through, split-core remanence results, after 20-mT AF demagnetization, from Hole 1042A.

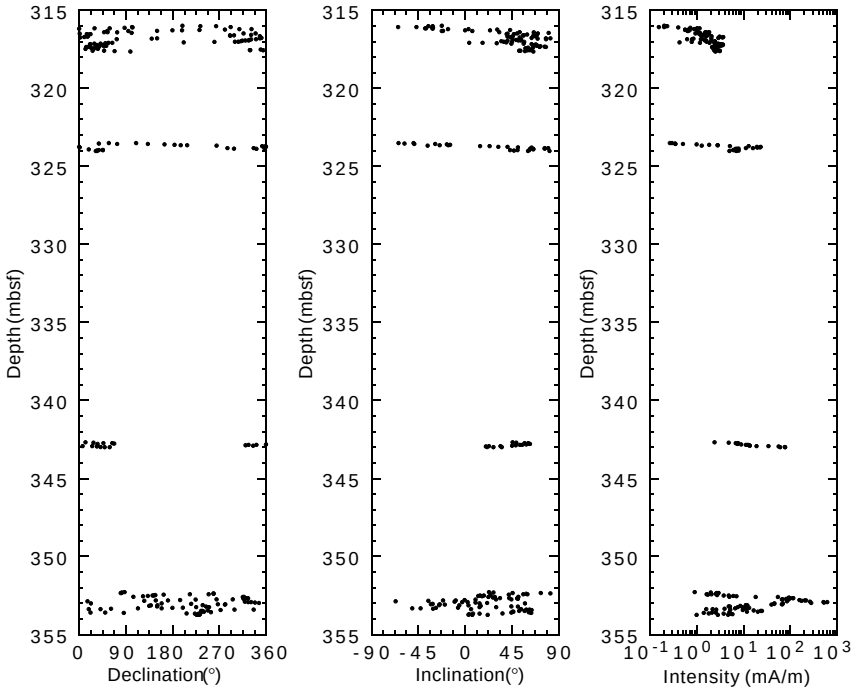

Figure 15. Pass-through, split-core remanence results, after 20-mT AF demagnetization, from Hole 1042B.

tems, this high-Ca concentration is among the highest reported in the drilling program, including at hydrothermal sites. At the Izu-Bonin sites, where Ca concentrations reach 155 mM at Site 792 and extreme values of 290–300 mM in the center of the Izu-Bonin sedimentary basin, the pore waters are otherwise chemically distinct and are characterized by salinities and chlorinities that are considerably higher than seawater. The origin of the high-Ca, low-Cl fluid at this site is not simply caused by low temperature, closed-system hydration reactions of volcanogenic sediments as at the Izu-Bonin sites. Dehydration reactions, which require moderate to elevated temperatures, are also involved at this open-system site. Mg concentrations decrease with depth; therefore the Mg/Ca values decrease as well (Figs. 17B, 17C).

Silica concentrations show a sharp change in gradient at the fault zone depth interval, increasing steadily below 100 mbsf (Fig. 17D). Because only 0.5- to 1.0-ml pore fluid was recovered at depths greater than 230 mbsf, the deeper samples were not analyzed for silica concentrations.

Sediment and Igneous Rock Results

Inorganic Carbon, Organic Carbon, and Total Sulfur

The results of inorganic and organic carbon, calcium carbonate, nitrogen, and sulfur analyses in the sediments at Site 1042 are presented in Table 12.

Percentages of calcium carbonate ($CaCO_3$) were calculated from the IC concentrations, assuming that all of the carbonates are present as pure calcite. $CaCO_3$ concentrations range from 3.1 to 5.9 wt%. These values are similar to those measured at Site 1041 (see "Geochemistry" section, "Site 1041" chapter, this volume).

Total organic carbon (TOC) contents range from 1.04 to 2.28 wt%. Total sulfur (TS) concentrations at Site 1042 vary between 1.0 and 1.6 wt% (Table 12). High sulfur concentrations probably reflect disseminated pyrite and pyrite nodules that are present in the core (see "Lithostratigraphy and Structures" section, this chapter). Total nitrogen (TN) varies between 0.19 and 0.24 wt%. TOC/TN values of 6 to 11 suggest a dominance of marine organic matter.

X-ray Fluorescence Analyses of the Solid Phases

A sparse set of samples was recovered from the intermittently cored intervals at Site 1042 for XRF analysis to provide a basic characterization of the siliciclastic sediments from Unit 1, both above 240.1 mbsf and below 353.6 mbsf. A more detailed sample set was taken from the sedimentary and igneous clasts in the breccias of Unit 2 (316.0–353.6 mbsf) to further constrain the nature of the materials making up the high-velocity layer beneath the prism and possibly the basement of the Costa Rica prism.

Major element analyses for the siliciclastic sediments and the igneous clasts from the breccia are reported in Table 13. Trace element analyses are reported for the siliciclastic sediments, carbonate-cemented sedimentary clasts, and igneous clasts in Table 14.

Figure 18 shows the variation with depth of SiO_2, Fe_2O_3*, TiO_2, Ba, and Cr. The sparse set of data points for the siliciclastic sediments at Site 1042 shows a restricted range of compositions for these elements; a similarly limited compositional range is seen for other elements in Tables 13 and 14. The one sample analyzed to date from Unit 1 sediments beneath the breccia, at 362 mbsf, is essentially identical to the Unit 1 sediments recovered from above the breccia. The composition of the Site 1042 sediments is within the restricted range of variation observed for the sedimentary wedge at Site 1040, although this similarity may be an artifact of the sparse data set at Site 1042.

The high carbonate content of the sedimentary clasts from the breccias of Unit 2, Cores 170-1042B-1R though 3R, precluded the preparation of fusion beads for major element analyses. Trace element data, however, show signatures expected for relatively clean sandstones cemented with abundant carbonate (see "Lithostratigraphy and Structures" section, this chapter). Nb concentrations are below detection limits, and Zr contents are low (<28 ppm), arguing against significant heavy-mineral concentrations in the sandstones. Rb, Zn, Cu, Ni, and V contents are typically a factor of 5 lower in the sandstones than in the claystones, suggesting little admixture of clay or hydrous oxides to the sandstones. Sr contents are generally high, as a corollary to the carbonate cementation.

Four samples were taken from the breccia interval 343.2–353.5 mbsf, composed of a matrix plus carbonate and basaltic clasts (343.2 mbsf), a basaltic clast (352.7 mbsf), a mixture of basalt plus chert and carbonate (353.0 mbsf), and a mafic clast (353.5 mbsf; see "Lithostratigraphy and Structures" section, this chapter). The basaltic clast least mixed with other material has low TiO_2, Nb, and Zr, and relatively high Ba in comparison to other incompatible element abundances. These collectively form an arc signature that is different from that of the gabbros recovered at Sites 1039 and 1040. The mafic clast from 353.5 mbsf does indeed have a unique chemistry. Figure 18E shows the extremely high Cr content (1184 ppm) of this clast, and Table 14 shows extremely high Ni concentrations (584 ppm) as well. The major element chemistry, however, is too rich in SiO_2 and Al_2O_3 and has MgO contents too low to characterize this sample as ultramafic. Post-cruise electron microprobe studies will be required to show if this chemistry is a result of mixing between ultramafic material, clay, and chert fragments, or if this type of clast is cumulate rather than ultramafic in nature. The Zr/Nb value of this clast is in the range reported for the Costa Rican volcanoes. The chemistry of the igneous clasts is generally consistent with the derivation of the breccia from upslope materials.

Table 9. Composition of headspace gases at Site 1042.

Core, section, interval (cm)	Depth (mbsf)	C_1 (ppmv)	C_2 (ppmv)	C_3 (ppmv)	C_1/C_2
170-1042A-					
1R-1, 0-5	48.73	7,214	8	1	902
2R-2, 0-5	97.63	15,317	15	5	1,021
3R-1, 0-5	153.73	356,147	444	52	802
4R-2, 0-5	203.23	257,460	368	106	700
5R-2, 0-5	212.83	128,238	219	70	586
6R-2, 0-5	222.43	79,666	138	42	577
7R-2, 0-5	232.04	38,615	62	14	623
170-1042B-					
8R-1, 0-5	381.23	3,238	10	7	324

Notes: C_1, C_2, and C_3 represent methane, ethane, and propane, respectively. ppmv = parts per million by volume.

This table also appears on the volume CD-ROM.

PHYSICAL PROPERTIES

Density and Porosity

Laboratory Measurements

Only general trends can be determined in the variation of laboratory physical properties measurements, because cores were taken only every 50 m down to 200 mbsf, and the remaining cores, in the intervals 200–230 and 317–362 mbsf, were incomplete because of poor recovery and core disturbance.

Wet bulk densities of extracted core specimens (Fig. 1; Table 15) increase from 1.6 g/cm^3 at 50 mbsf to 1.8 g/cm^3 at 100 mbsf, whereas porosities decrease from 66% to 52% over the same interval. Densities and porosities generally remain at 1.8 g/cm^3 and 50%, respectively, down to the maximum drilled depth. However, over the interval

Table 10. Results of vacutainer gas analyses.

Core, section, interval (cm)	Depth (mbsf)	C_1 (ppmv)	C_2= (ppmv)	C_2 (ppmv)	C_3 (ppmv)	*i*-C_4 (ppmv)	*n*-C_4 (ppmv)	*i*-C_5 (ppmv)	*n*-C_5 (ppmv)	*i*-C_6 (ppmv)	*n*-C_6 (ppmv)	C_1/C_2
170-1042A-												
3R-2, 15-16	155.36	837,897	19	988	116	40	5	12	ND	5	1	848
4R-2, 15-16	203.36	723,706	ND	792	292	79	4	6	1	4	ND	914
5R-1, 50-51	213.31	236,078	ND	390	112	47	2	4	1	ND	ND	605
7R-2, 5-6	232.06	71,203	ND	110	22	10	1	8	ND	1	ND	647

Notes: C_1 = methane, C_2= = ethylene, C_2 = ethane, C_3 = propane, C_4 = butane, C_5 = pentane, C_6 = hexane; iso- and normal configurations of butane, pentane and hexane are designated as *i* and *n* prefixes; C_1/C_2 = methane/ethane ratio. ND = not determined.

from 310 to 350 mbsf, wet bulk density jumps to 2.5–2.6 g/cm^3 and porosity falls to 10%–20%. Grain densities are also larger in this interval, with values of 2.7–2.75 g/cm^3 compared to 2.6 g/cm^3 elsewhere. Gamma-ray attenuation (GRA) bulk densities (Table 16) show a similar trend in the specimen-based values, although the maximum value reached in the interval from 315 to 355 mbsf is only 2.0–2.1 g/cm^3. The interval of high densities and low porosities corresponds to the breccias of lithologic Unit 2 (see "Lithostratigraphy and Structures" section, this chapter). The deeper zone of reduced densities corresponds to the silty claystone of Unit 3.

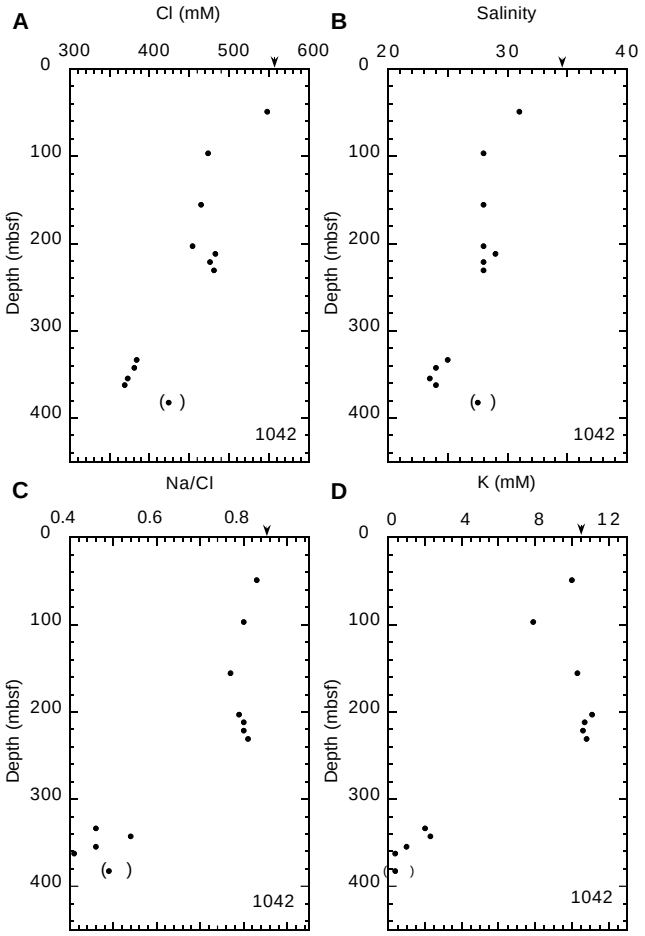

Figure 16. Concentration depth profiles of (**A**) Cl, (**B**) salinity, (**C**) Na/Cl, and (**D**) K. Arrows = seawater composition.

Natural Gamma Ray

Core Measurements

Natural gamma-ray measurements on unsplit cores indicate uniform values near 30 counts per second (cps; Fig. 19A; Table 17).

Downhole Measurements

In situ natural gamma-ray measurements were collected by CDR in Hole 1042C (Table 18; Fig. 20). The logs respond to mineralogic composition and therefore indicate changes in lithology.

Total spectral gamma-ray values range from 30 to 60 cps throughout the logged interval. Large negative excursions down to 20 cps from the baseline (40 cps) occur in intervals 55–65 and 65–73 mbsf. The negative excursions coincide with those of the resistivity log. A small positive excursion in total spectral gamma ray (up to 70 cps) and uranium yields (up to 4 ppm) occurs in the interval from 120 to 140 mbsf. Potassium yields show significant increase with depth at about 75 mbsf, which corresponds to the depth of an inferred normal fault.

P-wave Velocity

Measurements were made on extracted core specimens using the PWS3 transducer (Fig. 19B; Table 19). It was possible to measure representative samples of the major lithologies recovered, although trends with depth cannot be established. Data values fall into two main categories, values near 2000 m/s or in the range 4000–5000 m/s. The high velocities in the interval 210–230 mbsf were measured on limestone nodules or limestone interbeds within the clayey siltstone of lithologic Subunit 1B. The deeper zone of high velocities from about 310 to 350 m/s corresponds to the breccias of Unit 2. Velocities below this zone return to 2000 m/s, corresponding to the silty claystone of Unit 1B*.

Magnetic Susceptibility

Magnetic susceptibility (Fig. 1; Table 20) is uniformly low down to a depth of 340 mbsf. A zone of very high magnetic susceptibility from 342 to 355 mbsf corresponds closely to the breccia of Subunit 2B, which contains clasts of doleritic basalt.

Electrical Resistivity

LWD equipment, which included the CDR tool, was deployed at Site 1042C to a depth of 298 mbsf. LWD tools are typically configured with the CDN tool connected to a CDR. At Site 1042C, the CDN was not deployed because of the large diameter stabilizers that have been determined to exacerbate drilling problems in this geolog-

Table 11. Pore-fluid chemical data for major and minor constituents, Site 1042.

Core, section, interval (cm)	Depth (mbsf)	Volume (cm^3)	pH	Alkalinity (mM)	Salinity	Cl (mM)	SO_4 (mM)	Mg (mM)	Ca (mM)	K (mM)	Na (mM)	Si (µM)	Na/Cl	Mg/Ca
WSTP		10	ND	ND	35.00	558	29.4	54.5	11.7	10.5	474	ND	0.85	4.66
1R-1, 22-37	49	8	ND	ND	31.00	548	0.0	36.5	5.5	10.0	454	769	0.83	6.59
2R-1, 62-82	96.82	24	7.98	6.19	28.00	474	0.0	26.5	16.9	7.9	379	250	0.80	1.57
3R-2, 20-40	155.5	11	ND	ND	28.00	465	0.0	23.5	23.9	10.31	360	511	0.77	0.98
4R-1, 105-126	202.86	14	7.54	7.37	28.00	454	0.0	17.2	25.2	11.1	358	689	0.79	0.68
5R-1, 24-39	211.62	10	ND	ND	29.00	483	0.0	17.1	27.2	10.6	384	642	0.80	0.63
6R-1, 0-20	221	14	7.63	8.28	28.00	476	0.0	16.8	26.1	10.6	380	742	0.80	0.64
7R-1, 0-20	230.60	18	7.64	6.70	28.00	481	0.0	14.8	26.5	10.8	388	659	0.81	0.56
170-1042B-														
3R-CC, 0-12	333.26	2	ND	ND	25.00	384	0.0	3.3	99.6	2.0	176	ND	0.46	0.03
4R-1, 0-5	342.75	1	ND	ND	24.00	381	0.0	4.5	82.6	2.3	204	ND	0.54	0.05
5R-CC, 14-16	354.72	0.5	ND	ND	23.50	373	0.0	3.2	96.1	1.0	173	ND	0.46	0.03
6R-1, 30-60	361.90	1	ND	ND	24.00	369	0.0	4.9	102.8	0.4	153	ND	0.41	0.05
8R-1, 110-150	382.30	1	ND	ND	27.50	424	0.0	5.6	101.6	0.4	209	ND	0.49	0.06
Surface seawater			ND	ND	ND	520	26.6	52.2	10.2	10.0	438	2	0.84	5.12

Note: ND = not determined.

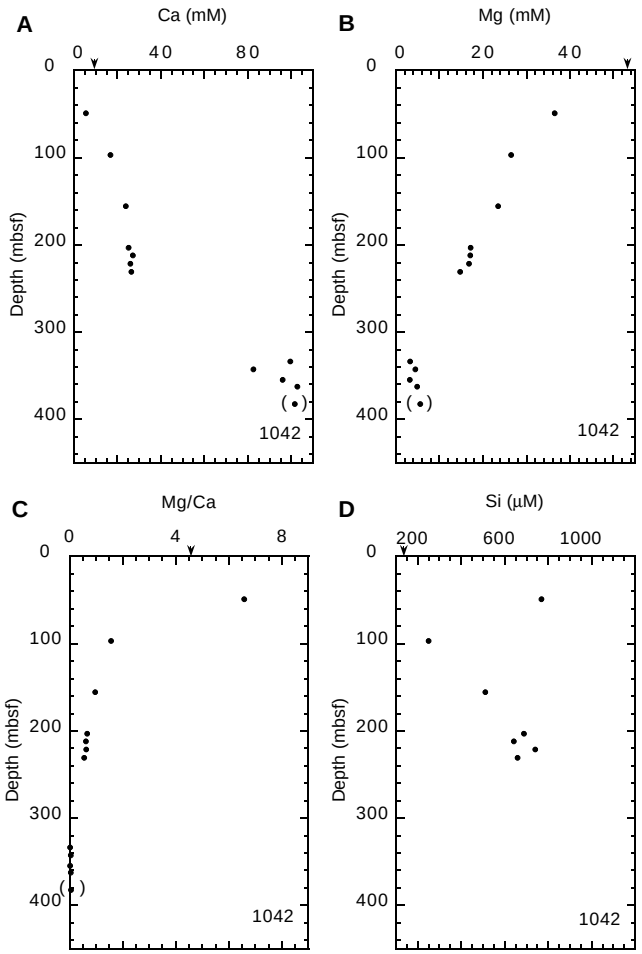

Figure 17. Concentration depth profiles of (**A**) Ca, (**B**) Mg, (**C**) Mg/Ca, and (**D**) silica. Arrows = seawater composition. The datum point in the parenthesis at the bottom of the figure is from the last core that included a large amount of rubble. This pore fluid is not truly representative of the designated depth and is not included in the discussion.

ic environment. The CDR tool was run to TD at a constant ROP of 25 m/hr to maximize data quality. Drilling was terminated at 298 mbsf when high torque and pump pressure were encountered. The deep and shallow resistivity logs are shown in Figure 20.

In the uppermost 67 mbsf, the resistivity values range from 0.8 to 1.5 Ωm. The log shows that a large negative excursion down to 0.4 Ωm occurs in the interval from 67 to 74 mbsf. This interval can be interpreted as a normal fault, as is also seen on the seismic-reflection profile (see "Background and Objectives" section, this chapter). The interval 0–74 mbsf is characterized by relatively low and fluctuated values of the shallow resistivity, suggesting borehole enlargement. From 74 to 145 mbsf, the resistivity values ranged from 1.8 to 2.4 Ωm. The shallow resistivity values show similar amplitudes to the deep resistivity, suggesting good borehole condition. A large increase of resistivity with depth occurs at 145 mbsf. Below 145 mbsf, the resistivity values gradually increase with depth from 2.3 to 3.2 Ωm. The interval from 145 to 295 mbsf is characterized by a number of small peaks. Because no significant responses in gamma-ray logs are identified in this interval, these peaks could be interpreted as high-resistivity hydrate layers.

Thermal Conductivity

Extreme disturbance and high induration of the recovered sediment precluded thermal conductivity measurements being made using the full-space method. It was therefore necessary to use the half-space technique. However, due to the paucity of intact blocks of sufficient size required for this technique, only four measurements were possible at sporadic intervals down the hole. Values range from 0.82 to 1.046 W/(m·K).

REFERENCES

Berrangé, J.P., and Thorpe, R.S., 1988. The geology, geochemistry, and emplacement of the Cretaceous–Tertiary ophiolitic Nicoya Complex of the Osa Peninsula, southern Costa Rica. *Tectonophysics*, 147:193–220.

Kuijpers, E.P., 1980. The geologic history of the Nicoya Ophiolite Complex, Costa Rica, and its geotectonic significance. *Tectonophysics*, 68:233–255.

Lallemand, S., and Le Pichon, X., 1987. Coulomb wedge model applied to the subduction of seamounts in the Japan trench. *Geology*, 15:1065–1069.

Lallemand, S., Malavieille, J., and Calassou, S., 1992. Effects of oceanic ridge subduction on accretionary wedges: experimental modeling and marine observations. *Tectonics*, 11:1301–1313.

Shipley, T.H., McIntosh, K.D., Silver, E.A., and Stoffa, P.L., 1992. Three dimensional seismic imaging of the Costa Rica accretionary prism: structural diversity in a small volume of the lower slope. *J. Geophys. Res.*, 97:4439–4459.

Taylor, B., Fujioka, K., et al., 1990. *Proc. ODP, Init. Repts.*, 126: College Station, TX (Ocean Drilling Program).

Ms 170IR-106

NOTE: Core-description forms ("barrel sheets") and core photographs can be found in Section 3, beginning on page 251. Smear-slide data and shore-based processed log data and descriptions can be found on CD-ROM. See Table of Contents for material contained on CD-ROM.

Table 12. Inorganic carbon, calcium carbonate, total carbon, total organic carbon, total nitrogen, total sulfur, and TOC/TN in sediments in Hole 1042A.

Core, section, interval (cm)	Depth (mbsf)	IC (wt%)	$CaCO_3$ (wt%)	TC (wt%)	TOC (wt%)	TN (wt%)	TS (wt%)	TOC/TN
170-1042A-								
1R-2, 32-33	49.39	0.37	3.1	1.45	1.08	0.19	1.20	6
2R-2, 33-34	97.25	0.38	3.1	1.42	1.04	0.19	0.99	5
3R-2, 16-17	155.36	0.60	5.0	2.14	1.54	0.24	1.04	6
4R-2, 33-34	203.29	0.55	4.6	2.10	1.55	0.25	1.60	6
5R-2, 33-34	212.33	0.80	6.6	3.08	2.28	0.21	1.12	11
6R-2, 33-34	221.43	0.71	5.9	1.86	1.15	0.21	1.52	5
7R-2, 32-33	231.02	0.70	5.8	2.01	1.31	0.21	1.26	6

Note: IC = inorganic carbon, $CaCO_3$ = calcium carbonate, TC = total carbon, TOC = total organic carbon, TN = total nitrogen, and TS = total sulfur.

This table also appears on the volume CD-ROM.

Table 13. Major element (XRF) analyses of siliciclastic sediments and igneous breccia clasts.

Core, section, interval (cm)	Sample type	Lithology	Depth (mbsf)	SiO_2	TiO_2	Al_2O_3	$Fe_2O_3^*$	MnO	MgO	CaO	Na_2O	K_2O	P_2O_5	Total	LOI
170-1042A-															
2R-1, 62-82	IWSJ	Sediment	96.72	61.27	1.12	17.25	9.65	0.058	4.01	1.61	2.31	2.296	0.144	99.70	8.10
3R-2, 20-40	IWSJ	Sediment	155.40	60.18	1.05	17.81	8.58	0.054	3.10	3.64	2.01	2.179	0.207	98.80	9.19
4R-1, 105-126	IWSJ	Sediment	202.75	59.88	0.97	18.02	8.23	0.050	2.83	4.64	2.17	1.828	0.209	98.79	8.81
5R-1, 24-39	IWSJ	Sediment	211.54	57.32	0.92	16.99	8.43	0.059	2.77	6.71	2.21	1.991	0.427	97.81	9.66
170-1042B-															
4R-1, 47-51	XRF	Breccia-igneous	343.17	57.56	1.17	11.93	7.95	0.172	3.25	13.91	1.46	1.930	0.159	99.48	14.34
5R-1, 37-39	XRF	Breccia-igneous	352.67	48.40	1.15	14.14	11.48	0.202	7.97	13.98	1.75	0.340	0.083	99.47	6.81
5R-1, 72-74	XRF	Breccia-igneous	353.02	63.90	0.39	5.17	7.81	0.145	2.52	16.19	0.48	0.171	0.653	97.42	10.23
5R-2, 9-11	XRF	Breccia-igneous	353.50	47.76	1.07	14.41	11.88	0.158	11.95	10.55	2.11	0.089	0.097	100.07	4.02
6R-1, 12-15	XRF	Sediment	362.02	61.20	1.01	17.78	8.80	0.046	2.37	4.97	1.24	1.172	0.204	98.78	8.57

Table 14. Trace element (XRF) analyses of siliciclastic sediments, carbonate-cemented sedimentary breccia clasts, and igneous breccia clasts.

Core, section, interval (cm)	Sample Type	Lithology	Depth (mbsf)	Nb	Zr	Y	Sr	Rb	Zn	Cu	Ni	Cr	V	Ce	Ba
170-1042A-															
2R-1, 62-82	IWSJ	Sediment	96.72	4.1	113.5	18.8	171.0	41.1	129	80	62	108	202	20	434
3R-2, 20-40	IWSJ	Sediment	155.40	4.5	110.8	17.1	258.0	36.8	113	49	33	71	163	19	584
4R-1, 105-126	IWSJ	Sediment	202.75	4.1	100.3	17.6	279.9	32.7	109	50	23	69	159	24	441
5R-1, 24-39	IWSJ	Sediment	211.54	4.0	98.9	20.1	367.5	33.6	97	36	23	74	151	18	538
170-1042B-															
1R-1, 29-31	XRF	Breccia-sediment	316.29	BDL	10.8	13.3	1217.6	2.0	22	12	6	55	24	6	93
1R-1, 48-50	XRF	Breccia-sediment	316.48	BDL	18.4	16.1	956.4	4.7	26	13	8	93	46	13	116
1R-1, 56-59	XRF	Breccia-sediment	316.56	BDL	18.9	20.1	1083.8	5.6	28	14	10	104	46	16	123
1R-2, 36-39	XRF	Breccia-sediment	317.43	BDL	27.7	16.2	803.4	9.6	26	15	8	66	35	7	199
2R-1, 9-11	XRF	Breccia-sediment	323.59	BDL	15.7	4.4	43.1	6.9	19	16	4	9	27	10	101
2R-1, 52-54	XRF	Breccia-sediment	324.02	BDL	13.8	23.3	683.4	4.7	33	14	9	82	32	24	118
4R-1, 47-51	XRF	Breccia-igneous	343.17	5.7	82.1	22.2	425.1	37.2	83	108	54	108	240	14	776
5R-1, 37-39	XRF	Breccia-igneous	352.67	3.0	53.2	18.6	180.5	2.9	73	133	109	202	297	13	124
5R-1, 72-74	XRF	Breccia-igneous	353.02	1.9	17.8	17.5	96.7	1.6	48	266	86	113	223	10	107
5R-2, 9-11	XRF	Breccia-igneous	353.50	1.9	50.3	21.3	94.3	2.5	112	159	549	1184	213	5	29
6R-1, 12-15	XRF	Sediment	362.02	5.6	109.3	19.0	276.0	30.1	132	72	37	58	174	27	352

Notes: All concentrations are in parts per million. IWSJ = interstitial water squeezecake split, XRF = picks from sampling table, BDL = below detection limit.

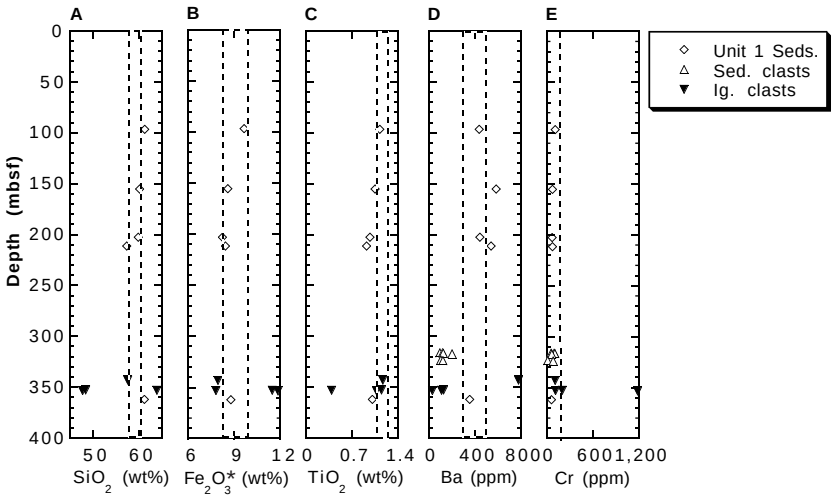

Figure 18. Concentration vs. depth of (**A**) SiO_2, (**B**) Fe_2O_3*, (**C**) TiO_2, (**D**) Ba, and (**E**) Cr. Dashed box indicates range of variation seen in the sedimentary wedge at Site 1040.

Table 15. Moisture and density data, and calculated phase relationships from discrete core specimens, Site 1042.

Leg	Site	Hole	Core	Type	Section	Top (cm)	Bottom (cm)	Depth (mbsf)	Beaker number	Beaker mass (g)	Beaker volume (g/cm^3)	Wet volume (g/cm^3)	Dry volume (g/cm^3)	Wet mass (g)	Dry mass (g)
170	1042	A	1	R	2	64	66	49.71	253	8.073	3.6365		6.11	19.14	14.581
170	1042	A	2	R	2	65	67	97.57	254	7.989	3.5986		6.99	20.66	16.945
170	1042	A	3	R	1	16	18	153.9	2	8.111	3.6536		6.82	20.037	16.33
170	1042	A	3	R	1	100	102	154.7	5	8.027	3.6158		6.93	20.374	16.67
170	1042	A	3	R	2	10	12	155.3	6	7.945	3.5788		7.2	21.377	17.41
170	1042	A	3	R	3	40	42	156	7	8.031	3.6176		7.32	21.592	17.59
170	1042	A	4	R	1	62	2	202.3	256	8.038	3.6207		6.41	17.952	15.13
170	1042	A	4	R	2	27	2	203.2	257	8.013	3.6095		7.06	20.451	16.797
170	1042	A	5	R	2	51	53	212.5	258	8.052	3.627		6.49	18.171	15.396
170	1042	A	5	R	1	64	66	211.9	260	8.213	3.6995		6.84	17.418	17.1

Table 15 (continued).

Leg	Site	Hole	Core	Type	Section	Top (cm)	Bottom (cm)	Depth (mbsf)	Water content (wet)	Water content (dry)	Wet bulk density (g/cm^3)	Dry bulk density (g/cm^3)	Grain density (g/cm^3)	Porosity (%)	Void ratio
170	1042	A	1	R	2	64	66	49.71	0.427	0.745	1.58	0.905	2.65	65.8	1.92
170	1042	A	2	R	2	65	67	97.57	0.304	0.436	1.79	1.24	2.65	53	1.13
170	1042	A	3	R	1	16	18	153.9	0.322	0.475	1.74	1.18	2.6	54.7	1.21
170	1042	A	3	R	1	100	102	154.7	0.311	0.451	1.76	1.22	2.62	53.5	1.15
170	1042	A	3	R	2	10	12	155.3	0.306	0.441	1.77	1.23	2.62	53	1.13
170	1042	A	3	R	3	40	42	156	0.306	0.441	1.76	1.22	2.59	52.7	1.11
170	1042	A	4	R	1	62	2	202.3	0.295	0.418	1.77	1.25	2.55	51	1.04
170	1042	A	4	R	2	27	2	203.2	0.304	0.438	1.75	1.22	2.55	52.2	1.09
170	1042	A	5	R	2	51	53	212.5	0.284	0.397	1.8	1.29	2.57	49.9	0.997
170	1042	A	5	R	1	64	66	211.9	0.0357	0.0371	2.66	2.57	2.83	9.3	0.102

This is a sample of the table that appears on the volume CD-ROM.

Table 16. Gamma-ray attenuation (GRA) bulk density data for Site 1042.

Leg	Site	Hole	Core	Type	Section	Top (cm)	Bottom (cm)	Depth (mbsf)	GRA density (g/cm^3)	Measured counts	Actual daq period (s)	Core diameter (cm)
170	1042	A	1	R	2	4.7	4.7	49.12	1.467	1.02E+05	5	6.7
170	1042	A	1	R	2	6.7	6.7	49.14	1.42	1.05E+05	5	6.7
170	1042	A	1	R	2	8.7	8.7	49.16	1.423	1.05E+05	5	6.7
170	1042	A	1	R	2	10.7	10.7	49.18	1.402	1.06E+05	5	6.7
170	1042	A	1	R	2	12.7	12.7	49.2	1.427	1.04E+05	5	6.7
170	1042	A	1	R	2	14.7	14.7	49.22	1.445	1.03E+05	5	6.7
170	1042	A	1	R	2	16.7	16.7	49.24	1.438	1.04E+05	5	6.7
170	1042	A	1	R	2	18.7	18.7	49.26	1.444	1.04E+05	5	6.7
170	1042	A	1	R	2	20.7	20.7	49.28	1.46	1.03E+05	5	6.7
170	1042	A	1	R	2	22.7	22.7	49.3	1.457	1.03E+05	5	6.7

Note: Daq = data acquisition.

This is a sample of the table that appears on the volume CD-ROM.

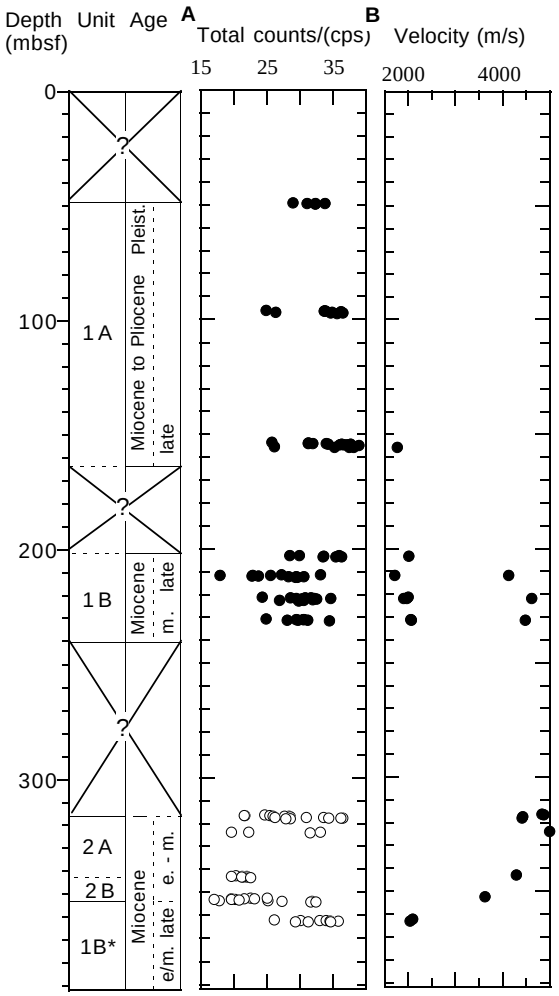

Figure 19. **A.** Natural gamma-ray radiation measured with the MST on cores from Site 1042. **B.** Acoustic *P*-wave velocity, measured by PWS3 transducers on specimens from split cores of Site 1042.

Table 17. Natural gamma-ray data obtained on unsplit core with the MST, Site 1042.

Leg	Site	Hole	Core	Type	Section	Top (cm)	Bottom (cm)	Depth (mbsf)	Total counts/s (cps)	Actual daq period (s)	Core diameter (cm)
170	1042	A	1	R	2	20.4	20.4	49.27	29	30	6.7
170	1042	A	1	R	2	30.4	30.4	49.37	32.33	30	6.7
170	1042	A	1	R	2	40.4	40.4	49.47	31.03	30	6.7
170	1042	A	1	R	2	50.4	50.4	49.57	33.77	30	6.7
170	1042	A	1	R	2	60.4	60.4	49.67	32.33	30	6.7
170	1042	A	2	R	1	10.4	10.4	96.2	24.87	30	6.7
170	1042	A	2	R	1	20.4	20.4	96.3	33.67	30	6.7
170	1042	A	2	R	1	30.4	30.4	96.4	33.93	30	6.7
170	1042	A	2	R	1	40.4	40.4	96.5	33.67	30	6.7
170	1042	A	2	R	1	50.4	50.4	96.6	36.2	30	6.7

Note: Daq = data acquisition.

This is a sample of the table that appears on the volume CD-ROM.

Table 18. Shipboard composite logging-while-drilling data from Hole 1042B.

Depth (mbrf)	Depth (mbsf)	ROP5 (m/hr)	ATR (Ωm)	PSR (Ωm)	RTIM (s)	GTIM (s)	GR (GAPI)	THOR (ppm)	URAN (ppm)	POTA (wt%)	CGR (cps)	SGR (cps)
3585.1	0.06	86.99	0.57	0.68	130	390	31.55	0.36	1.93	0.33	7.16	24.32
3585.2	0.21	435.83	0.65	0.75	140	400	40.43	0.47	2.48	0.4	8.68	30.72
3585.4	0.36	124.85	0.82	0.83	140	420	43.31	0.7	2.3	0.54	12.08	32.49
3585.5	0.51	137.36	0.84	0.95	150	440	49.97	0.73	2.87	0.55	12.28	37.72
3585.7	0.67	134.16	0.84	0.95	150	450	50.62	1.21	2.55	0.63	15.42	38.03
3585.8	0.82	169.5	0.87	0.85	160	480	51.53	1.47	2.19	0.76	18.68	38.1
3586	0.97	149.1	0.99	0.84	160	480	49.71	1.7	1.71	0.86	21.09	36.28
3586.1	1.12	120.26	1.01	0.73	190	480	50.36	2.24	1.3	0.95	24.69	36.23
3586.3	1.28	90.01	0.95	0.96	160	470	51.14	2.23	1.3	0.98	25.12	36.69

Note: ROP5 = 5-ft. averaged rate of penetration, ATR = attenuation resistivity, PSR = phase shift resistivity, RTIM = resistivity time after bit, GTIM = gamma ray time after bit, GR = gamma ray (GAPI), Thor = thorium, URAN = uranium, POTA = potassium, CGR = corrected gamma ray (thorium + potassium), and SGR = total gamma ray.

This is a sample of the table that appears on the volume CD-ROM.

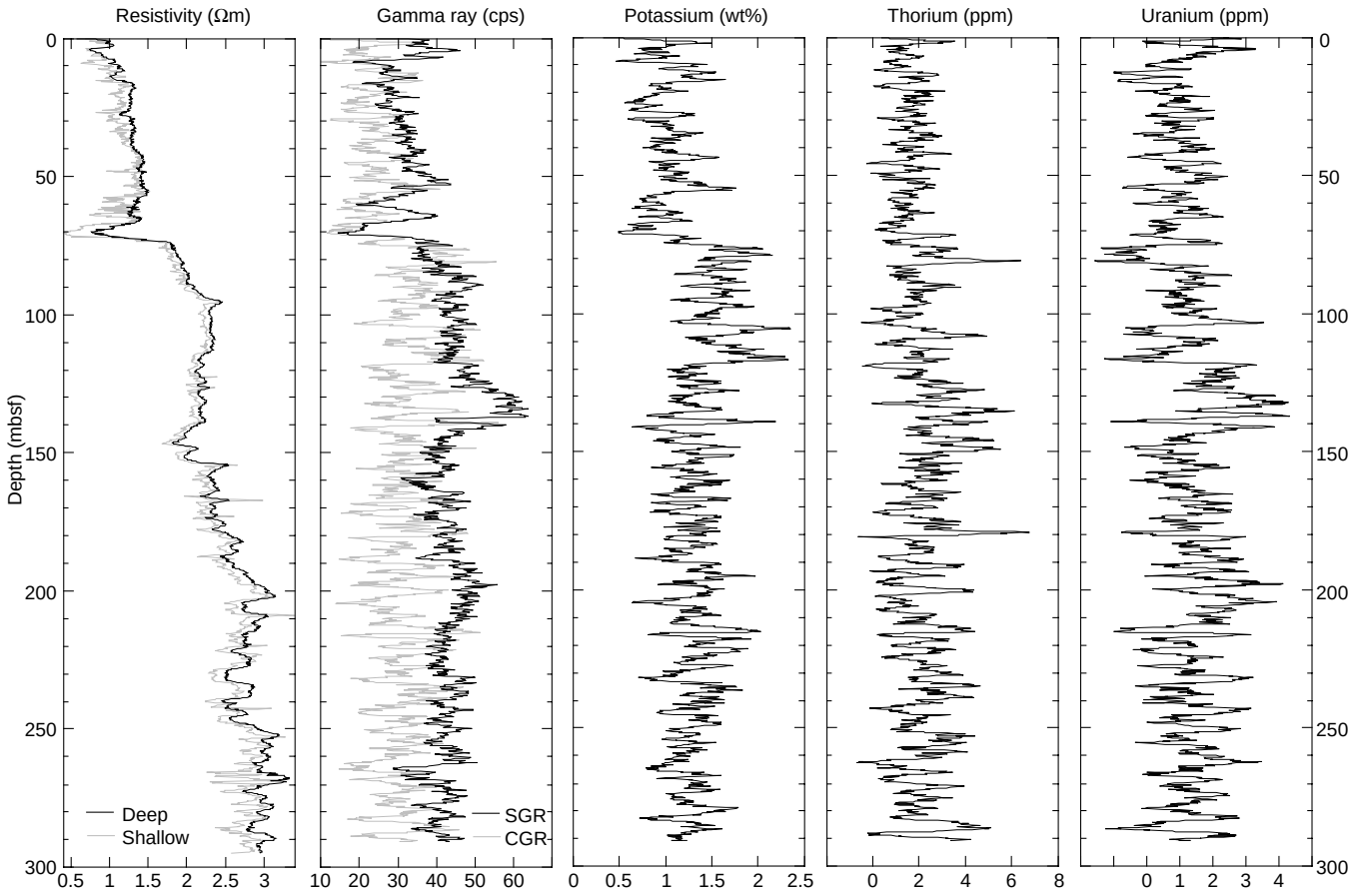

Figure 20. Summary of LWD at Hole 1042C. SGR = total spectral gamma ray; CGR = computed spectral gamma ray.

Table 19. *P*-wave velocities obtained from the PWS3 on split cores from Site 1042.

Leg	Site	Hole	Core	Type	Section	Top (cm)	Bottom (cm)	Depth (mbsf)	Velocity (m/s)
170	1042	A	3	R	3	20	20	155.8	1762.5
170	1042	A	4	R	2	57	57	203.53	2009.2
170	1042	A	4	R	2	57	57	203.53	2009.2
170	1042	A	5	R	1	57	57	211.87	1716
170	1042	A	5	R	1	57	57	211.87	4130.3
170	1042	A	6	R	1	39	39	221.29	1999.3
170	1042	A	6	R	1	107	107	221.97	1908.8
170	1042	A	6	R	2	72	72	221.82	1966.2
170	1042	A	6	R	2	76	76	221.86	4613.5
170	1042	A	7	R	2	76	76	231.46	4471.2
170	1042	A	7	R	2	55	55	231.25	2046.1
170	1042	A	7	R	2	70	70	231.4	2063.7
170	1042	B	1	R	1	40	40	316.4	4831.6
170	1042	B	1	R	1	74	74	316.74	4867.4
170	1042	B	1	R	2	38	38	317.45	4415.7
170	1042	B	1	R	2	94	94	318.01	4411.6
170	1042	B	2	R	1	25	25	323.75	4994.2
170	1042	B	4	R	1	25	25	342.95	4286.6
170	1042	B	5	R	1	25	25	352.55	3622.4
170	1042	B	6	R	1	25	25	362.15	2092.8
170	1042	B	6	R	1	114	114	363.04	2031

This table also appears on the volume CD-ROM.

Table 20. Magnetic susceptibility values obtained on unsplit cores using the MST, Site 1042.

Leg	Site	Hole	Core	Type	Section	Top (cm)	Bottom (cm)	Depth (mbsf)	Relative, drift corr. sus.	Relative, mean sus.	Actual daq period (s)	Core diameter (cm)	Sample elapsed zero time (s)	Drift correction
170	1042	A	1	R	2	4	4	49.11	25.8	25.8	5	6.7	8025	0
170	1042	A	1	R	2	6	6	49.13	26.2	26.2	5	6.7	11463	0
170	1042	A	1	R	2	8	8	49.15	26.2	26.2	5	6.7	14890	0
170	1042	A	1	R	2	10	10	49.17	25.8	25.8	5	6.7	18310	0
170	1042	A	1	R	2	12	12	49.19	26.6	26.6	5	6.7	21722	0
170	1042	A	1	R	2	14	14	49.21	27.8	27.8	5	6.7	25154	0
170	1042	A	1	R	2	16	16	49.23	29.4	29.4	5	6.7	28595	0
170	1042	A	1	R	2	18	18	49.25	27.6	27.6	5	6.7	32032	0
170	1042	A	1	R	2	20	20	49.27	26	26	5	6.7	35442	0
170	1042	A	1	R	2	22	22	49.29	25.8	25.8	5	6.7	38851	0

Note: Corr. = corrected, sus. = susceptibility, and daq = data acquisition.

This is a sample of the table that appears on the volume CD-ROM.

Previous Chapter Table of Contents Next Chapter